

It is shown that under an applied electric field, 180° ferroelectric domains act as elastic domains due to the converse piezoelectric effect. The effective dielectric and piezoelectric responses of thin films are determined by interdomain elastic interactions in addition to the substrate clamping effects. Characteristics of the piezoelectric loops of thin ferroelectric films have been explained from this point of view.

Experimental proof of the existence of strong interdomain elastic interactions has been obtained via piezoresponse force microscopy. It has been demonstrated that new 90° elastic domains are observed in epitaxial PZT 20/80 ($x=0.2$) thin films in vicinity of 180° domains, which are formed under strong local electric field created by the AFM tip. The area of internal stress arises under a conductive tip due to opposite signs of the converse piezoelectric strains in the switched 180° domain and the unswitched film. The formation of 90° domains leads to the relaxation of the internal stress. The necessary conditions for realization of this relaxation mechanism are presented.

While most of studies on piezoresponse of thin films are based on the assumption that the substrate is rigid, we have found that elasticity and thickness of the substrate play a significant role in the converse piezoresponse of the films and therefore cannot be neglected. Through the theoretical analysis based on different boundary conditions, it has been shown that the elastic deformation of the substrate contributes positively to the total piezodisplacement, while the film/substrate bending can give much larger negative deflections.

EFFECTS OF ELECTRIC FIELD ON PIEZOELECTRIC RESPONSES OF
FERROELECTRIC THIN FILMS

By

LANG CHEN

Dissertation submitted to the Faculty of the Graduate School of the
University of Maryland, College Park, in partial fulfillment
of the requirements for the degree of
Doctor of Philosophy
2005

Advisory Committee:
Professor Alexander L. Roytburd, Chair
Professor Manfred Wuttig
Professor Ichiro Takeuchi
Associate Professor Ray Phaneuf
Professor John Melngailis

© Copyright by
Lang Chen
2005

Acknowledgements

I would like to thank my advisor professor A. L. Roytburd for providing me with an excellent research opportunity. His enthusiasm, dedication and the drive for excellence in any task undertaken has been one of the primary motivating factors in this dissertation. With his vast experience in thermodynamics, interactions and discussions with him have been most useful and educational. I have learned and used from the models and concepts that he proposed regarding the elastic interactions between polydomains and the role of constraints in thin films.

I would also like to thank Professor R. Ramesh, for providing me with an excellent opportunity to cooperate with his group during the course of my graduate studies. It is a great honor for me to have been a part of his team that is at the forefront of research in oxide thin film materials. His devotion to research and his endless energy has affected everybody in his group including me as well.

I would like to thank the members of my Ph.D. defense committee, Profs. Manfred Wuttig, Ichiro Takeuchi, Ray Phaneuf from the Dept. of Materials Science and Engineering and Prof. John Melngailis from the Dept. of Electrical Engineering for their time and effort in reading through this rather elaborate text and for suggestions and encouragement.

I would like to thank my group members, Jun Ouyang, Jianhua Li, Zhengkun Ma for their inspiring discussions and encouragements.

I would like to thank Dr. V. Nagarajan and C. S. Ganpule for their help in the piezoresponse microscopy. The cooperation with them and all the other people in

professor Ramesh's group has been important to my knowledge and understanding of experimental results.

Finally I thank my family members and friends, all of them. This dissertation is dedicated to them. And I would like to acknowledge the funding received from National Science Foundation under DMR Grant No. 0210512 to support this work.

Table of Contents

Acknowledgements.....	ii
Table of Contents.....	iv
List of Tables	vi
List of Figures.....	vii
Chapter 1: Introduction.....	1
1.1 Ferroelectric and Piezoelectric Materials.....	2
1.2 Definitions and Notations in Thermodynamics	3
1.3 Outline of this Dissertation	7
Chapter 2: Nonlinear electric field dependence of piezoresponse in epitaxial ferroelectric lead zirconate titanate thin films	10
2.1 Introduction.....	10
2.2 Experiment results	13
2.3 Electric field dependence of piezoreponse of bulk single crystal ferroelectrics	15
2.4 Nonlinear thermodynamic theory and electric field dependence in PZT thin films	20
2.5 Comparison with experimental results for PZT films.....	23
2.6 Conclusion	28
Chapter 3: 180° ferroelectric elastic domains under electric field.....	29
3.1 Introduction.....	29

3.2 Elastic interactions in 180° ferroelectric domains and their effects on dielectric and piezoelectric responses.....	30
3.3 Discussion of dielectric and piezoelectric hysteresis loops	37
3.4 Effects of elastic interactions on switching in thin films	43
3.5 Conclusion	45
Chapter 4: Formation of 90° elastic domains during a local 180° switching in epitaxial ferroelectric thin films.....	46
4.1 Introduction.....	46
4.2 Experiment observations.....	48
4.3 Thermodynamic estimations.....	52
4.4 Conclusion	59
Chapter 5: Contribution of substrate to converse piezoelectric response of constrained thin films	60
5. 1: Introduction.....	60
5. 2: Thin film/substrate couple	62
5.3: Conclusion	66
Chapter 6: Summary	67
Appendix: Piezoresponse Force Microscopy.....	69
References.	72
Glossary of notations.....	82

List of Tables

Table 1: Values of parameters of the free energy expansions for various PZT compositions at 25° C	16
Table 2: Extrinsic dielectric constants of PZT and BaTiO ₃	36
Table 3: Thermodynamic coercive fields for bulk and thin films (misfit=0).....	45
Table 4: Data used to the estimation of necessary condition of relaxation of piezostress through new elastic domain formation.....	57

List of Figures

Figure 1.1: Perovskite $\text{Pb}(\text{Zr}_x\text{Ti}_{1-x})\text{O}_3$ crystal structure illustrating two polarization states with the Ti^{4+} (Zr^{4+}) ion shifted (A) up and (B) down with respect to the oxygen octahedral. Figure adapted from Ref. 7.....	1
Figure 1.2: The relations between the thermal, electrical and mechanical properties of a crystal. Figure adapted from Ref. 3	4
Figure 1.3: Summary of piezoelectric equations in matrix notations.....	7
Figure 2.1: Polarization-electric field hysteresis loops of BaTiO_3 thin film capacitors (200 nm) grown by PLD on GdScO_3 and DyScO_3 with SrRuO_3 top and bottom electrodes. The inset shows the hysteresis loop of an unstrained bulk BaTiO_3 single crystal for comparison. Figure adapted from Ref. 17.....	12
Figure 2.2: d_{33} measured by piezoresponse force microscopy of epitaxial $\text{PbZr}_x\text{Ti}_{1-x}\text{O}_3$ thin films of composition (a) PZT 20/80, $x=0.2$; (b) PZT 40/60, $x=0.4$; and (c) PZT 50/50, $x=0.5$	14
Figure 2.3: Calculated nonlinear electric field dependences of piezoelectric coefficients in bulk crystal $\text{PbZr}_x\text{Ti}_{1-x}\text{O}_3$ with composition $x=0.0, 0.2, 0.4$ and 0.5 : (a) PT, (b) PZT 20/80, (c) PZT 40/60, (d) PZT 50/50.....	18
Figure 2.4: Calculated nonlinear electric field dependences of effective piezoelectric coefficients of PZT films: (a) PT, misfit $\varepsilon_M=0\%$, $S^P=3.4 \times 10^{-12} \text{ m}^2 \text{ N}^{-1}$ and $\xi_P=1.35$; (b) PZT 20/80, misfit $\varepsilon_M=0.5\%$, $\xi_P=1.3$, $S^P=4.0 \times 10^{-12} \text{ m}^2 \text{ N}^{-1}$; (c) PZT 40/60, misfit	

$\varepsilon_M=0.9\%$, $S^P=7.0 \times 10^{-12} \text{ m}^2 \text{ N}^{-1}$, $\xi_P=0.7$; (d) PZT 50/50, misfit $\varepsilon_M=1.2\%$,
 $S^P=9.0 \times 10^{-12} \text{ m}^2 \text{ N}^{-1}$, $\xi_P=0.6$25

Figure 2.5: Calculated nonlinear electric field dependences of piezoresponse of (a) PZT 20/80, the dark lines show the results of changing misfits from -1% , 0% , 0.5% to 1% when $S^P=4.0 \times 10^{-12} \text{ m}^2 \text{ N}^{-1}$; the shaded area plots the results of changing elastic compliances from $S^P=3.0$ to $7.0 (\times 10^{-12} \text{ m}^2 \text{ N}^{-1})$ at fixed misfit value of 0.5% ; and of (b) PZT 50/50, the dark lines show the results of changing misfits from 0% to 1.2% when $S^P=9.0 \times 10^{-12} \text{ m}^2 \text{ N}^{-1}$; the shaded area are the results of changing compliances from $S^P=6.0$ to $12.0 (\times 10^{-12})$ when we fix misfit at 1.2% . Both experimental data in Figure 2.5 (a) and (b) are plotted in line and circles.....27

Figure 3.1: 180° domains and piezostress under electric field.....30

Figure 3.2: Dependence of Polarization, piezoelectric and dielectric constants on the applied electric field of an ideal single domain film.....32

Figure 3.3: Dependence of polarization, piezoelectric and dielectric constants on the applied electric field for a thin film consisted of 180° ferroelectric domains, including extrinsic effects due to domain wall movement. The two peaks at the left bottom are corresponding to the extrinsic contribution in dielectric measurement. The circled areas in the right bottom are “noses” of piezoelectric hysteresis loop which corresponding to the extrinsic contribution.36

Figure 3.4: Experiment measurements of a 50 nm PZT 20/80 film.....41

Figure 3.5: Analysis of the extrinsic effects of a 50 nm PZT 20/80 thin films.....42

Figure 4.1: (a) A reversed 180° domain under a AFM tip, (b) Piezostarin of the 180° domain under electric field, (c) Relaxation of piezostrain through formation of new

90° domains. (d) After the field is turned off, 90° domains expand through the film and form a stable configuration.....47

Figure 4.2: Piezoresponse force microscopy measurements of domain images for 1 mm thick PZT 20/80 films deposited on STO/Si and STO substrates.....49

Figure 4.3: (a) PFM domain structure image, (b) PFM image after a local switching with a -12V pulse for one second at site marked with '+' in (b), (c) Plan view diagram of new 90° domains formed and reversed 180° domain, (d) 3-D view diagram of new 90° domains formed and reversed 180° domain.....51

Figure 4.4: (a) PFM image after a positive local switching with a +12V pulse for one second at site marked with '+', no new 90° domains were formed. (b) New 90° domain was formed near the same site marked with '+' with a reversed 180° domain.....52

Figure 4.5: 3-dimesional polydomain structures in epitaxial films. Picture adapted from Ref. 80.....53

Figure 5. 1: Different boundary conditions of a thin film (h) on a much thicker substrate (H): (a) Fixed bottom and side surfaces of the substrate; (b) Bending of two-layer plates consisting of a piezoelectric thin film and a substrate, initial state of the film and substrate (left) and the thin film and substrate under the electric field along z coordinates (right); (c) A symmetrical three-layer film/substrate/film stack (left), corresponding to the fixed bottom surface of the substrate (right).....61

Figure A.1: Schematic illustration of the principle behind piezoresponse microscopy. Domains poled oppositely (a) and (b) vibrate out of phase for the same sinusoidal input (c)(Adapted from Ref. 98).....69

Figure A.2: Schematic diagram of the AFM setup for measuring piezoelectric constants in ferroelectric thin films.....70

Figure A.3: Calibration of electromechanical constants with X-cut quartz.....70

Chapter 1: Introduction

Piezoelectricity is a fundamental process of electromechanical interaction and is usually a representative of linear coupling in energy conversion.¹ More than a century has passed since Pierre Curie first discovered the piezoelectric effect in 1880. This effect has wide applications in electrical engineering field such as transducers, filters, sensors and actuators.¹⁻⁶ Compared with conventional piezoelectric materials such as quartz, Rochelle salt, KH_2PO_4 (KDP), relatively new ferroelectric materials including BaTiO_3 , $\text{Pb}(\text{Zr}_x\text{Ti}_{1-x})\text{O}_3$ can provide much stronger piezoelectric effect, LiNbO_3 and LiTaO_3 can be used in surface-acoustic-wave devices.^{4,5} With the trend of minimization of devices, thin films of ferroelectric materials has been intensely studied and used in microelectromechanical (MEMS) devices.⁷⁻⁸ In this chapter, the concepts of ferroelectricity and piezoelectricity will be introduced briefly, then the notations of basic thermodynamic relationships to describe both effects will be explained, finally the outline of this dissertation will be given.

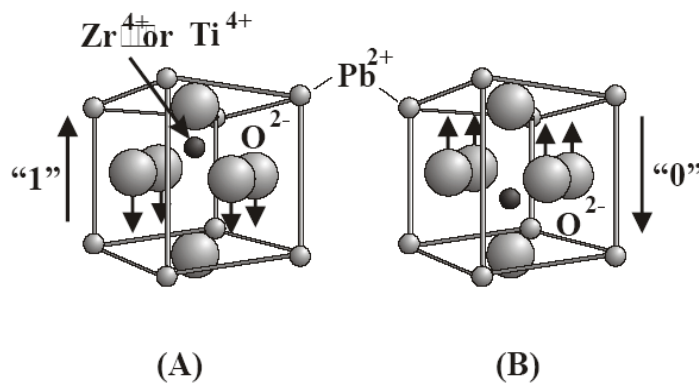


Figure 1.1: Perovskite $\text{Pb}(\text{Zr}_x\text{Ti}_{1-x})\text{O}_3$ crystal structure illustrating two polarization states with the Ti^{4+} (Zr^{4+}) ion shifted (A) up and (B) down with respect to the oxygen octahedral. Figure adapted from Ref. 7.

1.1 Ferroelectric and Piezoelectric Materials

A crystal is said to be ferroelectric when it has two or more degenerate orientation states in the absence of an electric field and can be shifted from one to another of these states by an applied electric field.^{4,5} Any two of the orientation states are identical in crystal structure and differ only in electrical polarization vector at null electric field. The polar character of the orientation states should represent an absolutely stable configuration in null field. To place the ferroelectric materials in perspective, consider the seven crystal systems: triclinic, monoclinic, orthorhombic, tetragonal, trigonal, hexagonal and cubic. These systems can be subdivided into point groups (crystal classes) according to their symmetry with respect to a point. There are 32 such crystal classes and 11 of them possess a center of symmetry, and therefore no polar properties. Of the remaining 21 noncentric crystal classes, all except one exhibit electrical polarity when subjected to mechanical stress (termed as the piezoelectric effect). Of the 20 piezoelectric crystal classes 10 are characterized by the fact that they have a unique polar axis.⁶ Crystals belonging to these classes are called polar because they possess a spontaneous polarization or electrical moment per unit volume. This spontaneous polarization is in general temperature dependent and the change of polarization with temperature is the pyroelectric effect. Only some of the pyroelectric crystals show a switchable polarization and these materials are termed ferroelectric. Ferroelectrics show a phase transition upon cooling through the Curie temperature T_c from a paraelectric phase above T_c (zero spontaneous polarization) to the ferroelectric phase below T_c . Below T_c , in the absence of applied field, there are at least two directions along which a spontaneous polarization can exist in a stable state. To

minimize depolarizing fields, different parts of the crystal orient their polarization vectors along any one of these degenerate directions. The resulting volume of uniform polarization within each of such regions is termed as a domain. The resulting domain structure usually leads to a near zero net polarization and the crystal needs to be poled in order to obtain a net spontaneous polarization.

The most commonly used ferroelectric materials today belong to the perovskite crystal structure.¹⁻⁷ The typical perovskite ABO_3 crystal structure is shown schematically in Figure 1.1. $PbTiO_3$ and $BaTiO_3$ are typical examples of perovskite ferroelectric crystals. In lead zirconate titanate [$Pb(Zr_xTi_{1-x})O_3$] for example, above T_c , the $Ti^{4+}(Zr^{4+})$ ions occupy the centers of each of the unit cells; the Pb^{2+} ions are located at the corners and the O^{2-} ions are centered on each of faces. In the distorted ferroelectric phase, there is a net dipole moment produced by the displacement up or down of the $Ti^{4+}(Zr^{4+})$ ions with respect to the other ions.⁷

1.2 Definitions and Notations in Thermodynamics

Phenomenological or macroscopic theories of dielectrics including ferroelectrics are used in this dissertation, which treat the materials as a continuum without regard to any underlying atomic structure. In general, fields are used in sufficient number to describe the elastic and dielectric properties of the macroscopic system, and the laws of thermodynamics and classical mechanics are used to obtain the relations between them. Phenomenological theory for ferroelectrics goes back to Ginzburg and Devonshire.¹⁻⁶ It is usually assumed possible to describe a dielectric system by three independent variables, chosen from the pairs (temperature, entropy), (stress, strain)

and (electric field, polarization). The couplings between them are shown in Fig 1.2 adapted from Nye's book.³ The concepts and notations are explained as below.

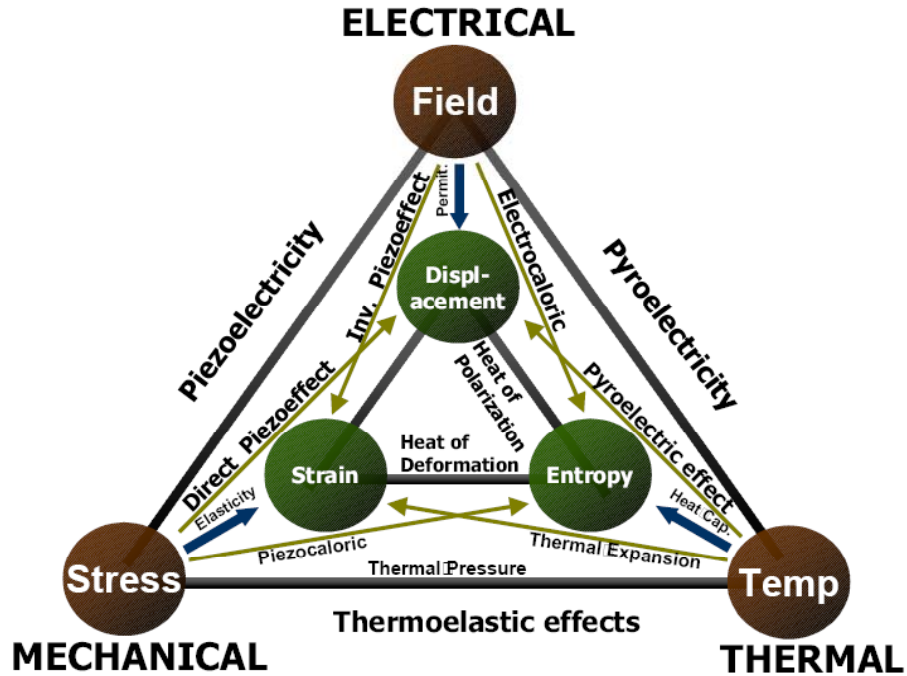


Figure 1.2 The relations between the thermal, electrical and mechanical properties of a crystal. Figure adapted from Ref. 3.

The following three vectors are introduced first: E the electric field intensity or field strength; P the polarization, that is the electric moment per unit volume

(or electric charge per unit area); and D , the electric displacement or electric flux density. The polarization of any crystal produced by an electric field is an anisotropic property, which can be represented by a second rank tensor, the dielectric susceptibility. Simple relationship between the electric displacement and the polarization under electric field can be written as

$$D = \kappa_0 E + P, \quad (1.1)$$

where κ_0 is a scalar constant, the permittivity of a vacuum, with the numerical value in m.k.s. units of 8.854×10^{-12} . In an anisotropic substance we have

$$P_i = \chi_{ij} E_j, \quad (1.2)$$

and for the dielectric constant, which is now also a tensor

$$\eta_{ij} = D / k_0 = \chi_{ij} / \kappa_0 + 1 \cong \chi_{ij} / \kappa_0, \quad (1.3)$$

since usually in ferroelectrics, $\eta_{ij} \gg 1$. It can be proven from energy considerations of symmetry, the dielectric properties of a crystal can be characterized by the magnitudes and directions of three principle dielectric constants or susceptibilities.³

If a stress is applied to certain crystals they develop an electric moment whose magnitude is proportional to the applied stress. This is known as the direct piezoelectric effect. Thus if a uniaxial tensile stress σ is applied along one of the diad axes of a quartz crystal, the magnitude of the electric moment per unit volume, or the polarization charge per unit area, is given by $P = d \sigma$. In general, we can relate the polarization and the stress as

$$P_i = d_{ijk} \sigma_{jk}, \quad (1.4)$$

where d_{ijk} are the piezoelectric moduli. The first term in this expression for P_i , for

example, would be written as:

$$P_i = d_{ij} \sigma_{ij}, \quad (1.5)$$

which has 9 components. The summation is taken over repetitive suffixes. So the coefficients d_{ijk} are a third rank tensor with 27 coefficients. In general $d_{ijk} = d_{ikj}$ due to symmetry in crystals, therefore there are only 18 independent components of this tensor. In simplified matrix notation, the tensor subscripts 11, 22, 33, 23(or32), 31(or13), 12(or21) correspond to matrix subscripts 1, 2, 3, 4, 5, 6 respectively, Eq. (1.4) can be rewritten as

$$P_i = d_{ij} \sigma_j \quad (i = 1, 2, 3; j = 1, 2, \dots, 6). \quad (1.6)$$

The array of d_{ij} can be written out as

$$\begin{pmatrix} d_{11} & d_{12} & d_{13} & d_{14} & d_{15} & d_{16} \\ d_{21} & d_{22} & d_{23} & d_{24} & d_{25} & d_{26} \\ d_{31} & d_{32} & d_{33} & d_{34} & d_{35} & d_{36} \end{pmatrix}. \quad (1.7)$$

When an electric field is applied to a piezoelectric crystal the shape of the crystal changes. This is known as the converse piezoelectric effect. It is found that there is a linear relation between the components of the electric field E_i and the components of the strain tensor ε_{ij} , which describes the change of shape. The coefficients connecting the field and the strain in the converse effect are the same as those connecting the stress and the polarization in the direct effect. If the direct effect is written out as $P_i = d_{ijk} \sigma_{jk}$, the converse effect is written as

$$\varepsilon_{jk} = d_{ijk} E_i. \quad (1.8)$$

We can therefore write, for example, ε_{11} as

$$\varepsilon_{11} = d_{111} E_1 + d_{211} E_2 + d_{311} E_3$$

$$\text{or } \varepsilon_1 = d_{11}E_1 + d_{21}E_2 + d_{31}E_3 \quad (1.9)$$

In a matrix notation, we have

$$\varepsilon_j = d_{ij}E_i \quad (i = 1, 2, 3; j = 1, 2, \dots, 6) \quad (1.10)$$

The scheme in Figure 1.3 summarizes the piezoelectric equations in the matrix notation. Read horizontally it gives the direct effect and read vertically it gives the indirect or the converse effect.³

		ε_1	ε_2	ε_3	ε_4	ε_5	ε_6
		σ_1	σ_2	σ_3	σ_4	σ_5	σ_6
E_1	P_1	d_{11}	d_{12}	d_{13}	d_{14}	d_{15}	d_{16}
E_2	P_2	d_{21}	d_{22}	d_{23}	d_{24}	d_{25}	d_{26}
E_3	P_3	d_{31}	d_{32}	d_{33}	d_{34}	d_{35}	d_{36}

Figure 1.3: Summary of piezoelectric equations in matrix notations.

1.3 Outline of this Dissertation

The results of theoretical and experimental studies of the piezoeffect in thin ferroelectric films constrained by substrates are presented in this dissertation. The elastic interactions between the film and the substrate has been calculated and proven to be a key factor in determining total piezoresponse of thin film.

In chapter 2, a thermodynamic theory is employed to explain the electric field dependence of piezoelectric properties of a single domain $\text{PbZr}_x\text{Ti}_{1-x}\text{O}_3$ (PZT)

material. The strong nonlinearity of converse piezoelectric coefficient under large external electric field is proven to be intrinsic both in bulk crystal and in epitaxial thin films of tetragonal PZT. The tunability of piezoelectric responses by an external electric field and its dependence on film/substrate misfit and elastic compliance of thin films are characterized quantitatively. The theoretical predictions are in good agreement with the experimental results of piezoresponse force microscopy.

In chapter 3, it is shown that under an applied electric field, 180° ferroelectric domains act as elastic domains due to the converse piezoelectric effect. The effective dielectric and piezoelectric responses of thin films are determined by the interdomain elastic interactions in addition to the substrate clamping effects. Characteristics of the piezoelectric loops of thin ferroelectric films have been explained from this point of view.

In chapter 4, experimental proof of the existence of strong interdomain elastic interaction has been obtained via piezoresponse force microscopy. It has been demonstrated that new 90° elastic domains are observed in epitaxial PZT 20/80 ($x=0.2$) thin films in vicinity of 180° domains that is formed under strong local electric field created by the AFM tip. The area of internal stress arises under the conductive tip due to the opposite signs of the converse piezoelectric strains in the switched 180° domain and the unswitched film. The formation of 90° domains leads to the relaxation of the internal stress. The necessary conditions for realization of this relaxation mechanism are presented.

While most of studies on piezoresponse of thin films are based on the assumption that the substrate is rigid, we have found that elasticity and thickness of the substrate

play a significant role in the converse piezoresponse of the films and therefore cannot be neglected. Through the theoretical analysis based on different boundary conditions in chapter 5, it has been shown that the elastic deformation of the substrate contributes positively to the total piezodisplacement, while the film/substrate bending can give much larger negative deflections.

In chapter 6, a summary of this dissertation is given.

In the appendix, the principles of piezoresponse force microscopy used in the experimental measurements of piezoresponse and domain structure imaging of the ferroelectric thin films are explained briefly. The author's publications list is attached in the end after the references.

Chapter 2: Nonlinear electric field dependence of piezoresponse in epitaxial ferroelectric lead zirconate titanate thin films

2.1 Introduction

Ferroelectric materials, which display large electromechanical interactions, have been used for many years in sensors, actuators and transducers. While most commercial electromechanical materials are based on linear piezoelectric mechanisms, nonlinear electromechanical interactions are of interest in engineering structures with tunable properties.⁹ In recent years, piezoelectric nonlinearity has been a key issue in better response control of high performance electromechanical devices. Efforts toward description of piezoelectric nonlinearity can be separated into approaches considering extrinsic and intrinsic contributions to the nonlinearity of piezoresponse. The extrinsic effect is focused on microscopic response taking into account extra contributions such as domain wall motion^{10,11}. The intrinsic effect usually includes introduction of some field dependence in the thermodynamical definition of the piezoelectric coefficient. Several descriptions of the intrinsic piezoelectric coefficient field dependence have been proposed either starting from the free energy equation, with field polynomial expansions^{10,12} or using empirical bias and amplitude dependence¹³ without any thermodynamical considerations. A field power law¹⁴ has been used in the description of domain wall depinning in the piezoceramics. Recently, a good qualitative result of the nonlinearity of piezoelectric response has been analyzed using the Preisach model of hysteretic systems as collections of distributed bistable units.¹⁵ On the other hand, a first principles

calculation on nonlinear electric field dependence of d_{33} and d_{31} in PbTiO_3 single crystal was published. The dependences of d_{33} on electric field of lead titanate were calculated, but the values of d_{33} and d_{31} were much smaller than experiment results for single crystal. This discrepancy was attributed to the choice of pseudopotentials in *ab initio* calculations.¹⁶

The piezoelectric response of ferroelectric PZT films has been extensively studied for years. The nonlinear effects caused by misfits in dielectric and piezoelectric constants at zero electric field or small electric field have been analyzed in detail. Enormous strains can exist in thin films when one material is deposited on another one, resulting from differences in crystal lattice parameters and thermal expansion behavior between the film and the underlying substrate or arising from defects formed during film deposition. As a result, the properties of thin films can be markedly different than the intrinsic properties of the corresponding unstrained bulk materials. Strain also offers the opportunity to enhance particular properties of a chosen material in thin film form, namely strain engineering. Strain engineering could facilitate large shifts in the paraelectric-to-ferroelectric transition temperature (T_c)^{17,18} and remanent polarization (P_r).¹⁸⁻²⁰

Figure 2.1 shows the ferroelectric hysteresis loops measured on the ferroelectric stacks grown on GdScO_3 and DyScO_3 substrates with 2000-Å-thick BaTiO_3 layers, together with results from a BaTiO_3 single crystal. The P_r and coercive field (E_c) were determined to be $\approx 50 \mu\text{C}/\text{cm}^2$ and 80 kV/cm for the fully coherent $\text{BaTiO}_3/\text{GdScO}_3$ sample and $\approx 70 \mu\text{C}/\text{cm}^2$ and 25 kV/cm for the partially relaxed $\text{BaTiO}_3/\text{DyScO}_3$ sample, respectively. This P_r value is almost 270% of the $26 \mu\text{C}/\text{cm}^2$ of single crystal

BaTiO₃, 3.5 times higher than the maximum switching charge density (20 μC/cm²) assumed in the scaling analysis of FeRAM, and comparable to the P_r of unstrained Pb(Zr,Ti)O₃ films. As this P_r of ~70 μC/cm² was observed in a partially relaxed sample with ϵ_s of -1.3%, a coherently strained BaTiO₃/DyScO₃ sample with ϵ_s of -1.7% could have an even higher P_r .¹⁷

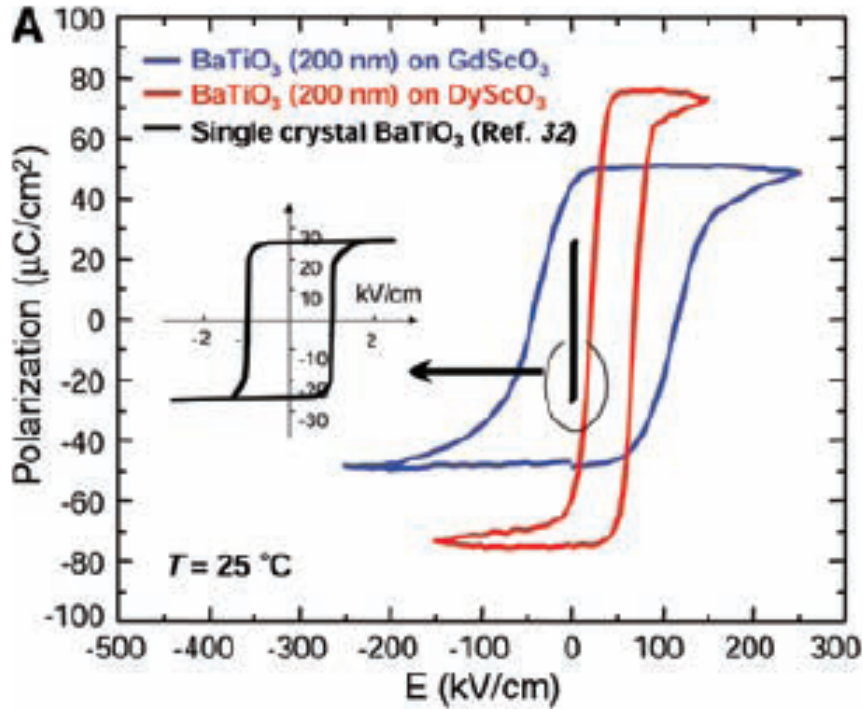


Figure 2.1: Polarization-electric field hysteresis loops of BaTiO₃ thin film capacitors (200 nm) grown by PLD on GdScO₃ and DyScO₃ with SrRuO₃ top and bottom electrodes. The inset shows the hysteresis loop of an unstrained bulk BaTiO₃ single crystal for comparison. Adapted from Ref. 17.

While the nonlinearity induced by misfit between thin films and thick substrate has been well understood,¹⁷⁻²⁰ the nonlinearity caused by large electric field has not. Due to relatively small thickness (100~200 nm) of thin films, the electric field can be as

large as 10^8 (V/m) inside the films. Therefore, the nonlinearity of piezoelectric coefficient vs. applied electric field is notable in thin films, which has been observed by many techniques including laser double-beam measurement,²¹ AFM²²⁻²⁵ and STM.²⁶

In this chapter, we use a thermodynamic approach²⁷ to describe the nonlinearity of piezoelectric response and obtain quantitative characteristics of its tunability by electric field both in bulk single crystals and in thin films. In addition, the results of theoretical calculations are verified by comparison with experimental data for PZT thin films.^{25,27}

2.2 Experiment results

Recent piezoresponse microscopy experiments demonstrate that the decrease of piezoelectric responses with increasing electric field, which can be as large as 20%-50%, depends on PZT compositions and the field strength. Epitaxial quality $\text{PbZr}_x\text{Ti}_{1-x}\text{O}_3$ ($x=0.2, 0.4$ and 0.5) films were grown on SrTiO_3 (STO) and STO/Si substrates with $\text{La}_{0.5}\text{Sr}_{0.5}\text{CoO}_3$ top and bottom electrodes by pulsed laser deposition (PLD). The epitaxial nature of these films as well as the absence of 90° domains has been proven via x-ray scans and TEM studies.²⁵ Figure 2.2 (a)-(c) shows the results obtained by piezoresponse scanning microscopy for epitaxial $\text{PbZr}_x\text{Ti}_{1-x}\text{O}_3$ thin films with $x=0.2, 0.4$ and 0.5 respectively. The dependences of d_{33} on the electric field i.e. the tunability of PZT 50/50($x=0.5$) and PZT 40/60($x=0.4$) are much larger than that of PZT 20/80($x=0.2$).

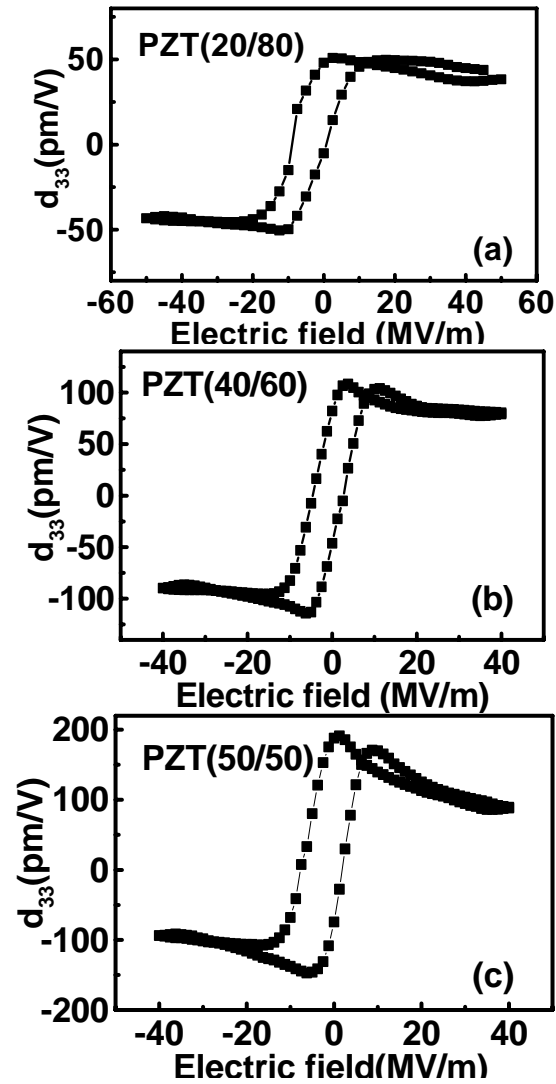


Figure 2.2: d_{33} measured by piezoresponse microscopy of epitaxial $\text{PbZr}_x\text{Ti}_{1-x}\text{O}_3$ thin films of composition (a) PZT 20/80, $x=0.2$; (b) PZT 40/60, $x=0.4$; and (c) PZT 50/50, $x=0.5$.

2.3 Electric field dependence of piezoreponse of bulk single crystal ferroelectrics

First, we consider a bulk single crystal or freestanding film composed of a single tetragonal domain under electric field E along polarization P . In the presence of top and bottom electrodes, depolarizing field can be neglected, and the Landau-Devonshire-type free energy^{28,29} can be written as:

$$G = a_1 P^2 + a_{11} P^4 + a_{111} P^6 - EP, \quad (2.1)$$

where a_1 , a_{11} , and a_{111} are the dielectric stiffness and higher-order stiffness coefficients at constant stress, E is electric field strength, and P is the polarization. The minimum of Eq. (2.1) gives an equilibrium polarization P under given field E . In bulk case, the polarization $P^b(E)$ is composed of two parts: spontaneous polarization P_0^b and induced polarization $p^b(E)$ [here the superscript b stands for bulk, and f for film; subscript 0 for zero electric field so P_0^b means spontaneous polarization of a bulk crystal].

$$P^b(E) = P_0^b + p^b(E), \quad (2.2)$$

$$(P_0^b)^2 = \frac{-a_{11} + (a_{11}^2 - 3a_1 a_{111})^{1/2}}{3a_{111}}, \quad (2.3)$$

The induced polarization $p^b(E)$ is field dependent. Similar to Ref. 22, we consider the ‘intrinsic’ static susceptibility $\chi^b(E) = \frac{dp^b(E)}{dE}$, excluding other extrinsic effects such as the contribution from the movement of 180° domain walls.

The longitudinal strain ε along c axis can be written as:

$$\varepsilon = Q_{11} P^2 = Q_{11} (P_0^b)^2 + 2Q_{11} P_0^b p^b(E) + Q_{11} [p^b(E)]^2, \quad (2.4)$$

where Q_{11} is the electrostrictive constant. The second term on the right hand of Eq. (2.4) is the piezostain term, and the third one is the electrostriction term. The electrostriction contribution in strong ferroelectrics usually is negligible compared with piezoelectric strain, i.e. their ratio:

$$\frac{Q_{11}[p^b(E)]^2}{2Q_{11}P_0^b p(E)} = \frac{p^b(E)}{2P_0^b} \quad (2.5)$$

is small. Calculation for PZT systems shows that the ratio in $\text{PbZr}_x\text{Ti}_{1-x}\text{O}_3$ ($x=0, 0.2, 0.4, 0.5$) is equal to 3.2% for PT, 4.3% for PZT 20/80, and 8.2% for PZT 40/60 at a field of 10^8 V/m; and 5.0% for PZT 50/50 at 5×10^7 (V/m)(The data we use for PZT crystals are listed in Table 2.1, adapted from Refs. 28-30).

Table 1: Values of parameters of the free energy expansions for various PZT compositions at 25° C

	$a_1(10^7$	$a_{11}(10^7$	$a_{111}(10^8$	$Q_{11}(10^{-2}$	$Q_{12}(10^{-2}$
	m/F)	$m^5/C^2F)$	$m^9/C^4F)$	$m^4/C^2)$	$m^4/C^2)$
PT	-17.08	7.253	2.606	8.900	-2.600
PZT 20/80	-14.84	-3.050	2.475	8.142	-2.446
PZT 40/60	-8.340	3.614	1.859	8.116	-2.950

Therefore we neglect the electrostriction term to calculate the piezoelectric coefficients. They are the derivatives of converse piezoelectric strain and can be expressed as:

$$d_{33}^b(E) = \frac{d(2Q_{11}P_0^b p(E))}{dE} = 2Q_{11}P_0^b \chi^b(E); \quad (2.6)$$

$$d_{31}^b(E) = \frac{d(2Q_{12}P_0^b p(E))}{dE} = 2Q_{12}P_0^b \chi^b(E). \quad (2.7)$$

These two relations show that the nonlinear effect of susceptibility gives rises to nonlinearity of piezoelectric coefficient in bulk PZT. Figure 2.3 (a)-(d) show these ‘intrinsic’ nonlinear electric field dependences of piezoelectric properties calculated for bulk crystal PZT. It’s obvious that there are much strong electric field dependences in PZT 40/60 and PZT 50/50 than those in PT and PZT 20/80 compositions.

In addition to the exact numerical solutions presented in Figure 2.3, it’s also possible to use an analytical approximation of $p^b(E)$ and $\chi^b(E)$. The equilibrium state of polarization under electric field can be obtained by minimizing the free energy Eq. (2.1):

$$\frac{dG}{dP} = 0 \Rightarrow E = 2a_1P + 4a_{11}P^3 + 6a_{111}P^5, \quad (2.8)$$

Here $P = P_0^b + p^b$, and taking into account $p^b \ll P_0^b$, we obtain the susceptibility χ_0^b in zero field given below:

$$\chi_0^b = (2a_1 + 12a_{11}(P_0^b)^2 + 30a_{111}(P_0^b)^4)^{-1}. \quad (2.9)$$

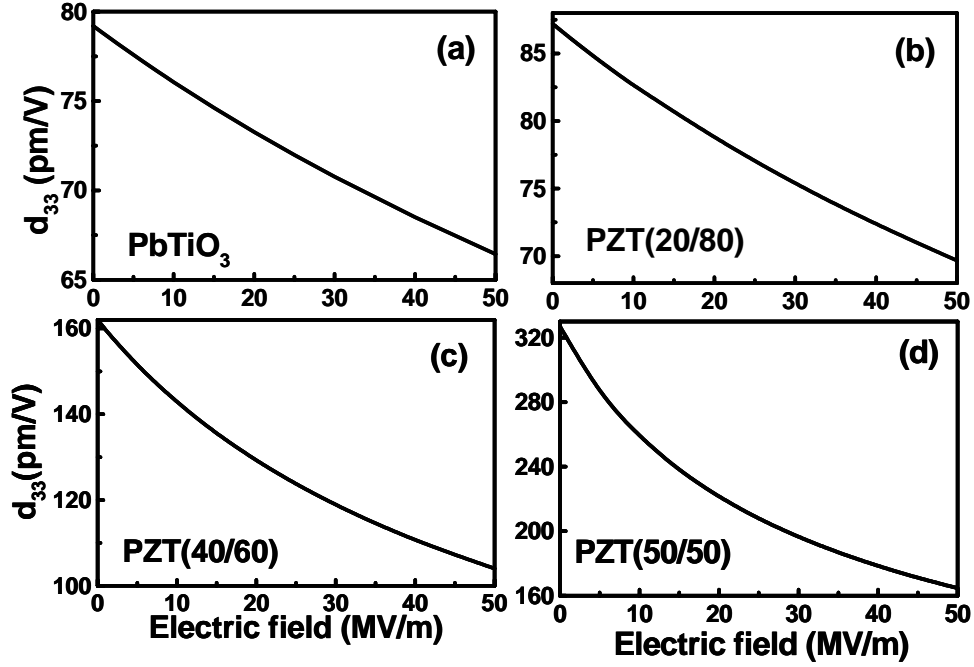


Figure 2.3: Calculated nonlinear electric field dependences of piezoelectric coefficients in bulk crystal $\text{PbZr}_x\text{Ti}_{1-x}\text{O}_3$ with composition $x=0.0, 0.2, 0.4$ and 0.5 :(a) PT, (b) PZT 20/80, (c) PZT 40/60, (d) PZT 50/50.

When the applied electric field is large enough, the calculation should include second order or even higher order approximation to have a more accurate description of the nonlinear part of dielectric susceptibility. Then Eq. (2. 8) can be expanded:

$$E(p) = \gamma_1 p + \gamma_2 p^2 + \dots \quad , \quad (2.10)$$

where $\gamma_1 = (\chi_0^b)^{-1}$ and $\gamma_2 = 12a_{11}P_0^b + 60a_{111}(P_0^b)^3$. We will see later that, comparing to experiment results, this second order approximation is good enough to describe nonlinear electric field dependence of piezoelectric properties. From this equation, we can get the field dependent susceptibility:

$$\chi^b(E) = \frac{dp(E)}{dE} = \frac{1}{(\gamma_1^2 + 4\gamma_2 E)^{1/2}} = \frac{\chi_0^b}{(1 + \lambda_b E)^{1/2}}, \quad (2.11)$$

$$\text{where } \lambda_b = \frac{4\gamma_2}{\gamma_1^2} = \frac{4[12a_{11}P_0^b + 60a_{111}(P_0^b)^3]}{[2a_1 + 12a_{11}(P_0^b)^2 + 30a_{111}(P_0^b)^4]^2}.$$

Using Eq. (2. 8) for E=0, λ_b is reduced to

$$\lambda_b = \frac{3P_0^b[a_{11} + 5a_{111}(P_0^b)^2]}{4[a_1 + a_{11}(P_0^b)^2]^2}. \quad (2.12)$$

Eqs. (2.6) and (2.7) then can be rewritten as:

$$\begin{aligned} d_{33}^b(E) &= 2Q_{11}P_0^b \chi^b(E) = 2Q_{11}P_0^b \frac{\chi_0^b}{(1 + \lambda_b E)^{1/2}} \\ d_{31}^b(E) &= 2Q_{12}P_0^b \chi^b(E) = 2Q_{12}P_0^b \frac{\chi_0^b}{(1 + \lambda_b E)^{1/2}} \end{aligned} \quad (2.13)$$

The parameter λ_b defines the tunability of dielectric and piezoelectric properties by electric field in bulk PZT. For PT and PZT 20/80, values of λ_b are only 8.419×10^{-9} and 1.133×10^{-8} (m/V); but for PZT 40/60 and 50/50, 2.851×10^{-8} and 5.892×10^{-8} (m/V). It shows the tunability in PZT 50/50 is nearly seven times larger than that in PT, five times larger than in PZT 20/80. For small field, Eq. (2.13) can be simplified as below:

$$d_{33}^b(E) = d_{33}^b(0) \left(1 - \frac{1}{2} \lambda_b E\right). \quad (2.14)$$

This equation shows a linear relationship of d_{33} with external DC electric field.

Depending on the values of λ_b the linear relationship [Eq. (2. 14)] is valid within a certain range of electric field for different compositions: for PT and PZT 20/80 less than 10^7 V/m; for PZT 50/50 less than 10^6 V/m. When the applied electric

field is beyond this range, strong nonlinear electric field dependences of piezoresponse should be taken into account.

2.4 Nonlinear thermodynamic theory and electric field dependence in PZT thin films

Consider a single domain thin epitaxial film oriented along (001) with direction of polarization P along [001] under external electric field E , which is constrained by a much thicker substrate. For this situation, the modified Landau-Ginzburg-Devonshire type free energy can be written as:

$$F = a_1 P^2 + a_{11} P^4 + a_{111} P^6 - EP + \frac{[\varepsilon_M - Q_{12}(P^2 - (P_0^b)^2)]^2}{S}, \quad (2.15)$$

where $S = S_{11}^P + S_{12}^P$, S_{ij}^P are the elastic compliances under constant polarization; P_0^b is the spontaneous polarization of the free standing film or bulk PZT; ε_M is the effective in-plane misfit, i.e. difference between in-plane lattice parameters of clamped and free-standing film; and Q_{12} is the in-plane electrostrictive constant. Therefore the previous results [Eq. (2.13), (2.14)], based on the description of free energy of bulk crystal or freestanding film, cannot be compared with experiment data of thin films deposited on thicker substrates. By modifying the coefficients in the expression for the free energy described in Eq. (2.15):

$$\alpha = 2\left(a_1 - \frac{2(\varepsilon_M + Q_{12}(P_0^b)^2)Q_{12}}{S}\right), \quad (2.16)$$

$$\beta = 4\left(a_{11} + \frac{Q_{12}^2}{S}\right), \quad (2.17)$$

$$\alpha_3 = 6a_{111} \quad , \quad (2.18)$$

Eq. (2. 15) is reduced to:

$$F = \frac{1}{2}\alpha P^2 + \frac{1}{4}\beta P^4 + \frac{1}{6}\alpha_3 P^6 - EP + \frac{(\varepsilon_M + Q_{12}(P_0^b)^2)^2}{S} . \quad (2.19)$$

The equilibrium $P(E)$ follows from $\frac{dF}{dP} = 0$,

$$E = \alpha P + \beta P^3 + \alpha_3 P^5 . \quad (2. 20)$$

The spontaneous polarization of constrained film P_0^f when $E=0$, follows:

$$P_0^f = \sqrt{\frac{-\beta + (\beta^2 - 4\alpha\alpha_3)^{1/2}}{2\alpha_3}} \quad (2. 21)$$

Introducing the field-induced polarization $p = P^f(E) - P_0^f$, it's possible to solve Eq.

(2. 20) and get an exact numerical solution. The zero field susceptibility can be obtained from approximation of Eq. (2. 20), taking into account the first term only,

$$E = (\alpha + 3(P_0^f)^2 \beta + 5(P_0^f)^4 \alpha_3)p \quad , \quad (2. 22)$$

$$\chi_0^f = \frac{dp}{dE} = (\alpha + 3(P_0^f)^2 \beta + 5(P_0^f)^4 \alpha_3)^{-1} . \quad (2. 23)$$

If the second order terms are taken into account, Eq. (2. 20) reduces to:

$$E = \gamma_1 p + \gamma_2 p^2 , \quad (2. 24)$$

where $\gamma_1 = \alpha + 3(P_0^f)^2 \beta + 5(P_0^f)^4 \alpha_3 = (\chi_0^f)^{-1}$, $\gamma_2 = 3P_0^f \beta + 10(P_0^f)^3 \alpha_3$.

The solution is:

$$p = \frac{\sqrt{\gamma_1^2 + 4\gamma_2 E} - \gamma_1}{2\gamma_2} \quad , \quad (2. 25)$$

So

$$\chi^f(E) = \frac{dp}{dE} = \frac{1}{\sqrt{\gamma_1^2 + 4\gamma_2 E}} = \frac{\chi_0^f}{\sqrt{1 + \lambda_f E}}, \quad (2.26)$$

where

$$\begin{aligned} \lambda_f &= \frac{4\gamma_2}{\gamma_1^2} = \frac{4(3P_0^f \beta + 10(P_0^f)^3 \alpha_3)}{(\alpha + 3(P_0^f)^2 \beta + 5(P_0^f)^4 \alpha_3)^2} \\ &= \frac{P_0^f (3\beta + 10(P_0^f)^2 \alpha_3)}{(2\alpha + (P_0^f)^2 \beta)^2} \end{aligned} \quad (2.27)$$

The tunability factor λ_f depends on the modified thermodynamic coefficients in Eqs. (2.16)-(2.18), therefore it also depends on elastic compliance and misfit.

Due to the substrate-induced constraints,³¹ the effective longitudinal piezoelectric strain of the film can be written as:

$$\varepsilon_3^f(E) = Q_f (P^f(E)^2 - (P_0^b)^2), \quad (2.28)$$

$$\text{where } Q_f = Q_{11} + \xi_P Q_{12}, \quad \xi_P = \frac{-2S_{13}^P}{S_{11}^P + S_{12}^P}.$$

Therefore the effective piezoelectric coefficient is equal to:

$$d_{33}^f(E) = \frac{d\varepsilon_3^f}{dE} = 2Q_f P^f(E) \chi^f(E) \quad (2.29)$$

By using approximation in Eq. (2.24), Eq. (2.29) can be presented as:

$$d_{33}^f(E) \cong 2Q_f \left(P_0^f + \frac{\sqrt{\gamma_1^2 + 4\gamma_2 E} - \gamma_1}{2\gamma_2} \right) \frac{\chi_0^f}{\sqrt{1 + \lambda_f E}} \quad (2.30)$$

$$= 2Q_f \left(P_0^f + \frac{2\chi_0^f E}{\sqrt{1 + \lambda_f E} + 1} \right) \frac{\chi_0^f}{\sqrt{1 + \lambda_f E}} \quad (2.31)$$

Similar to Eq. (2.6), the electrostriction part is negligible, so the effective d_{33} is

$$d_{33}^f(E) = \frac{2Q_f P_0^f \chi_0^f}{\sqrt{1 + \lambda_f E}}. \quad (2.32)$$

It can also be simplified as:

$$d_{33}^f(E) = 2Q_f P_0^f \chi_0^f \left(1 - \frac{1}{2} \lambda_f E\right) = d_{33}^f(0) \left(1 - \frac{1}{2} \lambda_f E\right), \quad (2.33)$$

when the applied electric field is relatively small just as in Eq. (2.14) for the bulk case.

2.5 Comparison with experimental results for PZT films

According to the theoretical analysis above, the electric field tunability of piezoresponse of constrained ferroelectric films, Eq. (2.27), depends on film-substrate misfit and elastic properties of the films. The misfit parameter ε_M can be measured by x-ray experimentally. There are a lot of experimental data on misfit of epitaxial PZT films on different substrates; some results have been presented. Using resonance methods, the elastic properties of PZT ceramics have been studied especially for compositions near morphotropic phase boundary.³² On the other hand, no enough information has ever been known on single crystal properties.³³ Gavriyachenko and Fesenko et. al.³⁴⁻³⁶ measured the elastic compliance constants of $\text{PbTiO}_3(\text{PT})$ single crystal, along with dielectric and piezoelectric constants. Recently, two groups, Li et al.³⁷ and Kalinichev et al.³⁸ reported measurements of the complete set of electromechanical properties for PT using the Brillouin light scattering technique. Useful information about PZT 50/50 has been obtained theoretically by first principle calculations.^{39, 40} However there still exist some large differences between the elastic properties and piezoelectric properties even for PT single crystal.

Facing these difficulties for calculation of the effective piezoelectric coefficients,

we use the estimation of elastic properties based on the available data.²⁷ By supposing a possible range of elastic properties, we can demonstrate this nonlinear behavior, though the data for elastic properties are not complete. For comparison with experimental data, the following values of compliances and ξ_P are used. For PT, $S_{11}^P=6.05$, $S_{12}^P=-2.65$, $S_{13}^P=-2.30(\times 10^{-12} \text{ m}^2 \text{ N}^{-1})$, $S^P=3.4 \times 10^{-12} \text{ m}^2 \text{ N}^{-1}$ and $\xi_P=1.35$; for PZT 20/80, we take $\xi_P=1.3$, $S^P=4 \times 10^{-12} \text{ m}^2 \text{ N}^{-1}$; for PZT 50/50, we take $S^P=9.0 \times 10^{-12} \text{ m}^2 \text{ N}^{-1}$, $\xi_P=0.6$. We estimate that $S^P=7.0 \times 10^{-12} \text{ m}^2 \text{ N}^{-1}$ for PZT 40/60, $\xi_P=0.7$.

Calculated results based on descriptions of Eq. (32) are plotted in Figure 2.4 (a)-(d). The in-plane misfit measured by X-ray for PZT 20/80 is 0.5%; for PZT 40/60, 0.7% ; and for PZT 50/50, 1.2%. PT films of zero misfits are also calculated in Fig. 3(a). The tunability factor λ_f of these films from PT to PZT 20/80, PZT 40/60 and PZT 50/50 are 4.643×10^{-9} , 9.323×10^{-9} , 3.774×10^{-8} , and $1.28 \times 10^{-7}(\text{m/V})$ respectively. The values of λ_f in PT and PZT 20/80 are smaller than corresponding values of bulk crystals, while the λ_f in PZT 40/60 and PZT 50/50 are larger than bulk values (note here the tunability in PZT 50/50 is two times larger than in bulk crystal), which means the large misfits in these samples play an important role. Additionally, if the misfit is large enough, a single domain state is unstable, thus the film will possibly form polydomain structures.

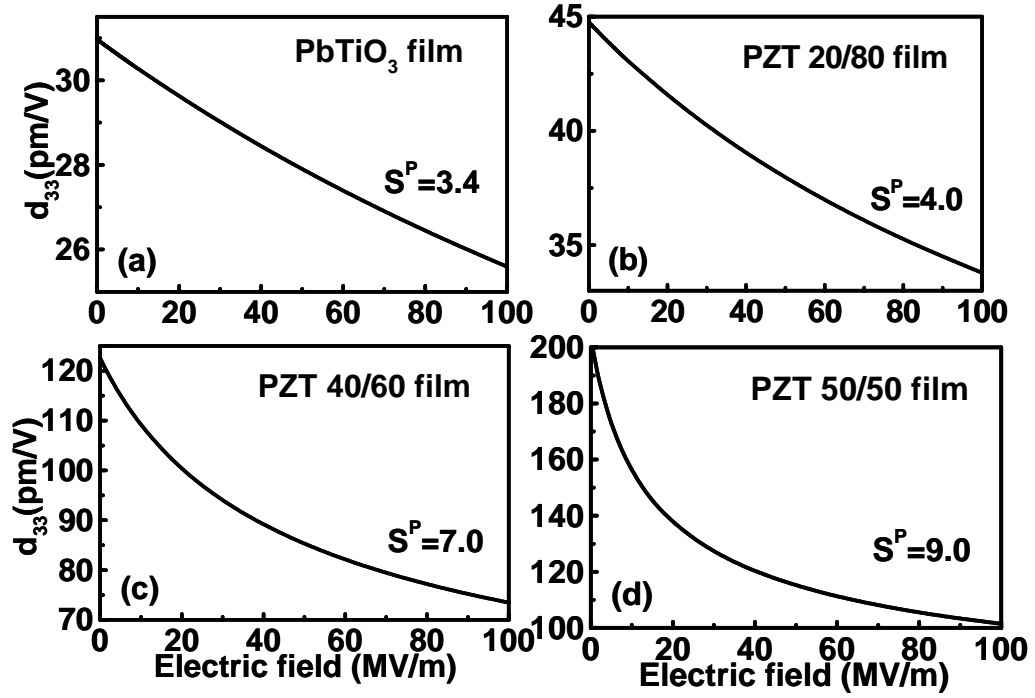


Figure 2.4: Calculated nonlinear electric field dependences of effective piezoelectric coefficients of PZT films: (a) PT, misfit $\varepsilon_M=0\%$, $S^P=3.4 \times 10^{-12} \text{ m}^2 \text{ N}^{-1}$ and $\xi_P=1.35$; (b) PZT 20/80, misfit $\varepsilon_M=0.5\%$, $\xi_P=1.3$, $S^P=4.0 \times 10^{-12} \text{ m}^2 \text{ N}^{-1}$; (c) PZT 40/60, misfit $\varepsilon_M=0.9\%$, $S^P=7.0 \times 10^{-12} \text{ m}^2 \text{ N}^{-1}$, $\xi_P=0.7$; (d) PZT 50/50, misfit $\varepsilon_M=1.2\%$, $S^P=9.0 \times 10^{-12} \text{ m}^2 \text{ N}^{-1}$, $\xi_P=0.6$.

In Figure 2.5, Eq. (2. 32) was used to plot the tunable curves of PZT 20/80 and 50/50 changes with the misfits, which indicates that adjusting misfit in PZT 50/50 could have more dramatic changes in tunability and relatively smaller ones in PZT

20/80. Figure 2.5 also shows the tunable d_{33} -E curves changes within the assumed ranges of elastic compliances. The corresponding tunability factor λ_f of PZT 20/80 is 8.669×10^{-9} and 1.022×10^{-8} (m/V) when compliance changes from 3.0×10^{-12} to 7.0×10^{-12} ($\text{m}^2 \text{N}^{-1}$); of PZT 50/50, 1.636×10^{-7} and 1.112×10^{-7} (m/V) when compliance changes from 6.0×10^{-12} to 12.0×10^{-12} ($\text{m}^2 \text{N}^{-1}$). Previous results for bulk PZT 20/80 and 50/50 show that the tunability factor is 1.133×10^{-8} (m/V) and 5.892×10^{-8} (m/V). By comparison, the tunability factor changes more when we change misfit than adjusting the compliance range, which means the uncertainty of compliance data is less important in determining the tunable factor compared to the effect of misfit. The theoretical results agree with the experimental result of PZT 20/80 and 50/50 films, which also demonstrates the validity of these assumed ranges of elastic compliances of PZT films.

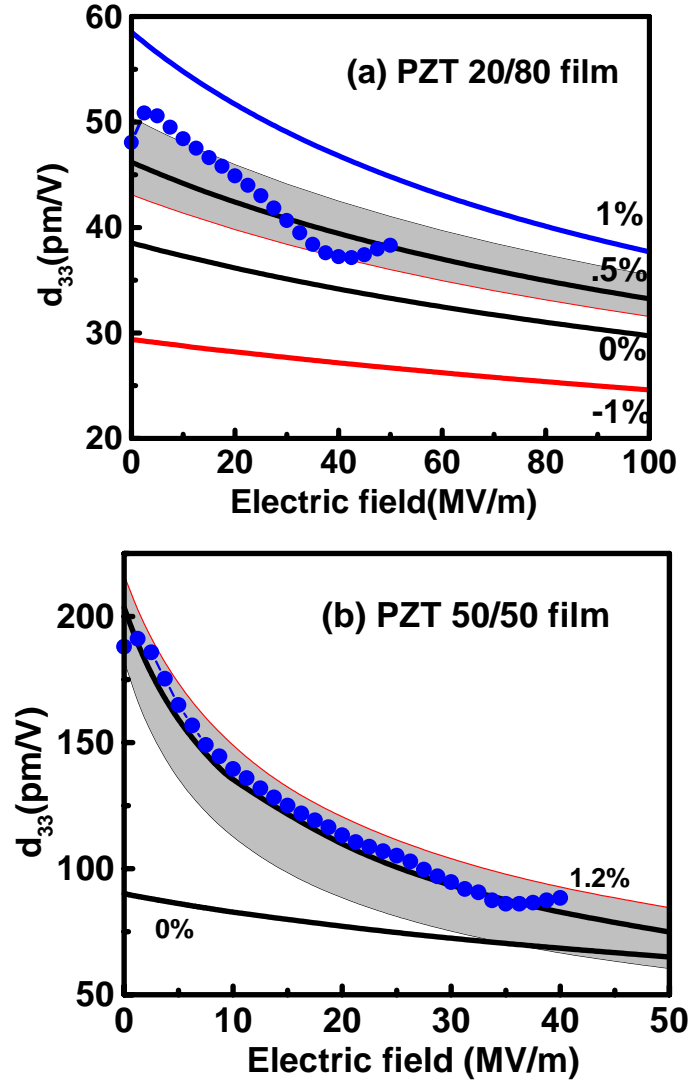


Figure 2.5: Calculated nonlinear electric field dependences of piezoresponse of (a): PZT 20/80, the dark lines show the results of changing misfits from -1% , 0% , 0.5% to 1% when $S^P=4.0 \times 10^{-12} \text{ m}^2 \text{ N}^{-1}$, the shaded area plots the results of changing elastic compliances from $S^P=3.0$ to $7.0 (\times 10^{-12} \text{ m}^2 \text{ N}^{-1})$ at fixed misfit value of 0.5% . (b): dark lines show the results of changing misfits from 0% to 1.2% when $S^P=9.0 \times 10^{-12} \text{ m}^2 \text{ N}^{-1}$; the shaded area are the results of changing compliances from $S^P=6.0$ to $12.0 (\times 10^{-12})$ when we fix misfit at 1.2% . Both experimental data in Fig.4 (a) and (b) are plotted in line and circles.

2.6 Conclusion

The thermodynamic study gives a theoretical explanation of nonlinear electric field dependence of intrinsic piezoelectric properties in single domain PZT crystal and epitaxial film. There are two regimes of the nonlinear behavior. In the relatively small field, linear electric field dependence in bulk single crystal

$$[d_{33}^b(E) = d_{33}^b(0)(1 - \frac{1}{2}\lambda_b E)] \text{ and thin films } [d_{33}^f(E) = d_{33}^f(0)(1 - \frac{1}{2}\lambda_f E)] \text{ is effective.}$$

Beyond this electric field range, more dramatic nonlinear relationship of electric field dependence dominates the change of piezoelectric properties. It is shown that the tunability is sensitive to misfit, thus it is possible to get different electric field tunabilities by adjusting misfits. The tunability can be controllable and enhanced through strain engineering, which has been reported dramatically increased ferroelectric qualities of epitaxial thin films.

Chapter 3: 180° ferroelectric elastic domains under electric field

3.1 Introduction

The stripe 180° domain structure appears in many fields of condensed matter system, such as ferromagnetics, ferroelectrics.⁴¹ Therefore, it is of great interest to understand and manipulate the various properties of these thin films in views of both sciences and engineering applications. Among them, 180° stripe ferroelectric domains,⁴¹⁻⁴⁴ with alternating polarizations between adjacent lamella in order to minimize the depolarization field, which has been well known to occur in bulk ferroelectric single crystals, ceramics and also observed in thin films recently, are important to the commonly used applications such as capacitors, memory cells, transducers, etc. In this chapter, a model in which 180° ferroelectric domains behave as elastic domains under an external electric field is proposed and its effect on the dielectric and piezoelectric responses is discussed. Specific features of piezoelectric hysteresis loops observed in ferroelectric thin films are explained based on this effect. The inter-domain and substrate clamping effect can inhibit the local switching constrained by substrate and surrounding domains when a large negative pulse is quickly applied to a single domain film. In addition, these clamping effects increase the coercive field by making local switching difficult through introducing 180° ferroelectric domain nuclei in thin films. The coercive field can reach the order of the theoretical value due to the thermodynamic instability for the single domain film under negative electric field when the film is ultra thin (the thickness is less than/ or in the order of 100 unit cells).

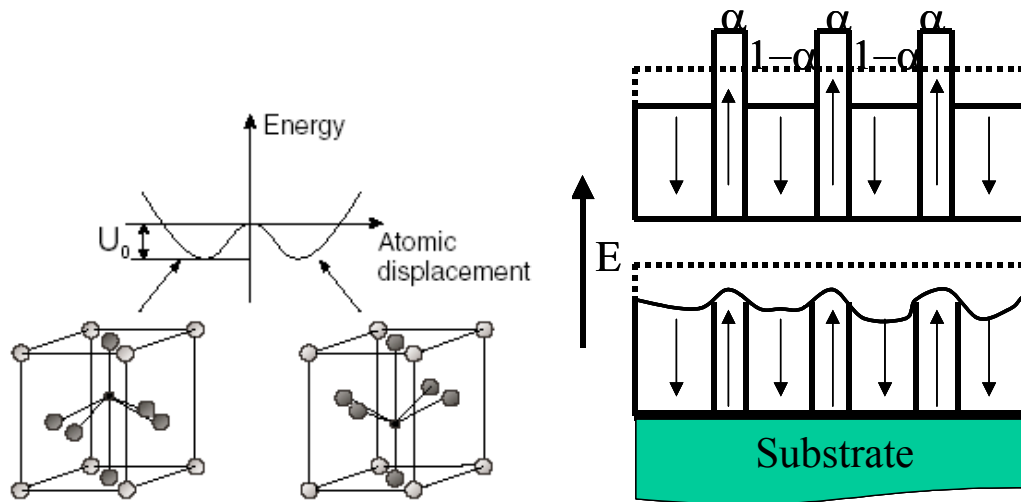


Figure 3.1: Illustration of 180° domains and piezostress under electric field.

3.2 Elastic interactions in 180° ferroelectric domains and their effects on dielectric and piezoelectric responses

180° ferroelectric domains are elastically identical in the absence of an electric field. But under an applied electric field, the converse piezoelectric strains in 180° domains have the opposite signs, one domain elongates while the other shrinks longitudinally. Due to the mechanical compatibility and the continuity of lattice across 180° walls, the difference of piezoelectric strains in the 180° domains is a source of internal stresses, which results in an interdomain clamping effect.⁴³⁻⁴⁵ On the other hand, in a thin film, both domains are also clamped by a much thicker substrate, which gives another constraint (Figure 3.1). For this point of view, 180°

domains act as elastic domains under electric field. The interdomain elastic interaction and the mechanical substrate clamping from the substrate are not negligible in considering the electromechanical properties of single crystals and thin films composed of 180° domains, especially in the thin film case when the external electric field is relatively large.

First let us briefly discuss the clamping of a single domain film on a thick substrate. As was discussed in chapter 2, the dielectric response and piezoelectric response are different with those of a freestanding film even there is no misfit between the thin film and the substrate. For the sake of simplicity, taking a linear approximation³³ of Eq. (2.15) and assuming the misfit of the film is zero, $P_0^f = P_0^b$, then by introducing the field induced polarization $p = P^f - P_0^b$, we can reduce Eq.

(2.15) to

$$F = \frac{p^2}{2\chi} + \frac{4Q_{31}^2 (P_0^b)^2 p^2}{S} - EP, \quad (3.1)$$

$$\text{or } F = \frac{p^2}{2\chi_f} - EP, \quad (3.2)$$

where

$$\frac{1}{2\chi_f} = \frac{1}{2\chi} + \frac{4Q_{31}^2 (P_0^b)^2}{S}, \quad (3.3)$$

χ_f is the effective dielectric susceptibility of the constrained zero-misfit film. The effective piezoelectric modulus of thin film clamped on substrate has a well-known relationship with that of freestanding film,³¹

$$d_{33}^f = d_{33} - \frac{2S_{13}}{S_{11} + S_{12}} d_{31}. \quad (3.4)$$

The electric field dependence²⁷ of polarization, piezoelectric effect and dielectric constant for single domain bulk/film were calculated in Chapter 2 and are shown as below (Figure 3.2).

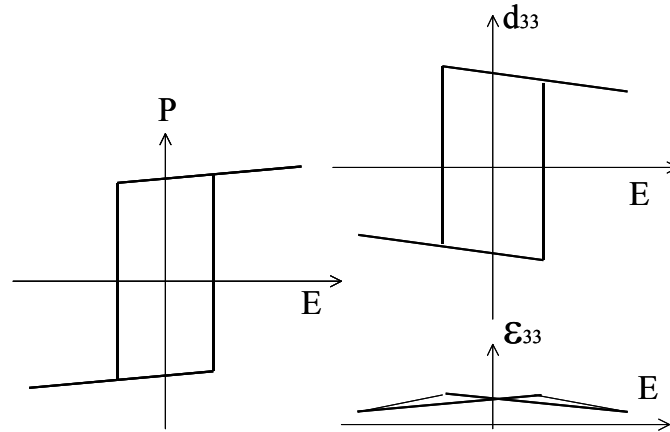


Figure 3.2: Dependence of polarization, piezoelectric and dielectric constants on the applied electric field for an ideal single domain film

For a constrained film composed of 180° domains in this study, here we do not discuss the initial formation process of 180° domains, which highly depends on the history of the sample, on many intrinsic and extrinsic factors. We just assume a period arrangement of stripe domains is formed with the switched domain volume fraction α and period D in a thin film of thickness h , with ideal top and bottom electrodes to compensate the polarization charges. Therefore, depolarization field is not considered. The substrate is assumed to be much thicker than the film and rigid. Assuming that domains are formed in a shape of vertical striped plates, the elastic energy due to the formation of 180° elastic domains can be calculated, following the

calculation of the equilibrium of polydomain structure in many works.⁴⁶⁻⁵⁹ The thermodynamic analysis presented below allows us to formulate the free energy of the stable domain structure under an applied electric field and to calculate the effective dielectric and piezoelectric responses of the ferroelectric thin films.

After an external electrical field E is applied, the piezoelectric strains are (due to the converse piezoelectric effect):

$$\hat{\eta} = \begin{bmatrix} 2Q_{31}P_s p_+ & 0 & 0 \\ 0 & 2Q_{31}P_s p_+ & 0 \\ 0 & 0 & 2Q_{33}P_s p_+ \end{bmatrix} \text{ for switched domains}$$

$$\hat{\theta} = \begin{bmatrix} -2Q_{31}P_s p_- & 0 & 0 \\ 0 & -2Q_{31}P_s p_- & 0 \\ 0 & 0 & -2Q_{33}P_s p_- \end{bmatrix} \text{ for unswitched domains, (3.5)}$$

where p_+ and p_- are the induced polarizations in the 180° switched and unswitched domains respectively, which are along the direction of the external field, P_s is the magnitude of spontaneous polarization at room temperature, which is equal to P_0^b for film with zero misfit, and Q_{31} and Q_{33} are the electrostrictive constants.

The free energy change of 180° domains under external field follows

$$F(\alpha, E) = \alpha \left(\frac{p_+^2}{2\chi} - p_+ E + \frac{4Q_{31}^2 P_s^2 p_+^2}{S} \right) + (1-\alpha) \left(\frac{p_-^2}{2\chi} - p_- E + \frac{4Q_{31}^2 P_s^2 p_-^2}{S} \right) + (1-2\alpha)P_s E + \alpha(1-\alpha)(e^{DI} - e^I) + \frac{\xi^* D \alpha^2 (1-\alpha)^2 e^I}{h} + Const \quad (3.6)$$

where

$$\begin{aligned}
e^{DI} &= \frac{S_{33}(\eta_{11} - \theta_{11})^2 + S_{11}(\eta_{33} - \theta_{33})^2 - 2S_{13}(\eta_{11} - \theta_{11})(\eta_{33} - \theta_{33})}{2(S_{11}S_{33} - S_{13}^2)} \\
&= \frac{2(S_{33}Q_{31}^2 + S_{11}Q_{33}^2 - 2S_{13}Q_{31}Q_{33})P_s^2}{(S_{11}S_{33} - S_{13}^2)}(p_+ + p_-)^2 = \frac{(p_+ + p_-)^2}{2k_{DI}}
\end{aligned} \tag{3.7}$$

is the direct elastic interaction between 180° switched and unswitched domains under the electric field, and

$$e^I = \frac{(\eta_{11} - \theta_{11})^2}{S} = \frac{4Q_{31}^2 P_s^2 (p_+ + p_-)^2}{S} = \frac{(p_+ + p_-)^2}{2k_I} \tag{3.8}$$

is the indirect elastic interaction between 180° domains through the substrate under the electric field. For D , the width of domain period and h , the thickness of thin film, note in Eq. (3.6), according to Roytburd's dense domain approximation^{52,53}:

$D < h$, ζ^* is a geometry parameter on the order of 1. If we consider a dense domain case, $D \ll h$ we may neglect the last two terms in Eq. (3.6) and rewrite it as

$$\begin{aligned}
F(\alpha, E) &= \alpha \left(\frac{p_+^2}{2\chi_f} - p_+ E \right) + (1 - \alpha) \left(\frac{p_-^2}{2\chi_f} - p_- E \right) \\
&+ (1 - 2\alpha) P_s E + \alpha(1 - \alpha) \frac{(p_+ + p_-)^2}{2k} + Const
\end{aligned} \tag{3.9}$$

where we set an effective elastic susceptibility using $\frac{1}{k} = \frac{1}{k_{DI}} - \frac{1}{k_I}$ (note $e^{DI} > e^I$ in most PZT and BT single crystals, see the calculated results listed in Table 2). The minimization of the free energy change in Eq. (3.9) with respect to p_+ and p_- gives

$$\begin{aligned}
\frac{dF(\alpha, E)}{dp_+} &= \frac{p_+}{\chi_f} - E + (1 - \alpha) \frac{(p_+ + p_-)}{k} = 0, \\
\frac{dF(\alpha, E)}{dp_-} &= \frac{p_-}{\chi_f} - E + \alpha \frac{(p_+ + p_-)}{k} = 0,
\end{aligned} \tag{3.10}$$

leads to

$$\begin{aligned}
p_+ &= \frac{\chi_f [k + (2\alpha - 1)\chi_f]}{\chi_f + k} E, \\
p_- &= \frac{\chi_f [k - (2\alpha - 1)\chi_f]}{\chi_f + k} E.
\end{aligned} \tag{3.11}$$

The induced polarizations in both domains are same ($p_+ = p_-$) only when $\alpha = 1/2$. In general, both induced polarizations p_+ and p_- are functions of domain fraction α , the effective dielectric susceptibilities of 180° domains are functions of domain fraction α too.

The total polarization of the film is

$$P_f = (1 - \alpha)P_- + \alpha P_+ = (2\alpha - 1)P_s + (1 - \alpha)p_- + \alpha p_+. \tag{3.12}$$

Thus the effective dielectric susceptibility is

$$\chi_{eff} = \frac{dP_f}{dE} = \frac{\chi_f [k + (2\alpha - 1)^2 \chi_f]}{\chi_f + k} + 2 \left(\frac{d\alpha}{dE} \right) \left[P_s + \frac{(2\alpha - 1)\chi_f^2 E}{\chi_f + k} \right]. \tag{3.13}$$

The first term in the right hand of Eq. (3.13) is the intrinsic contribution to dielectric response including the effects of substrate and interdomain elastic interactions, which is different from that of a single domain film [Eq. (3.3)]. The second term in the right hand of Eq. (3.13) is the extrinsic contribution due to the domain fraction changes under electric field. In most experimental measurements of dielectric constants, the extrinsic contribution is large compared with intrinsic part especially when the applied electric field is close to coercive field (Figure 3.3).

The effective out-of-plane strain is

$$\varepsilon_{eff} = (1 - \alpha)\varepsilon_- + \alpha\varepsilon_+ = 2Q_{33}^f P_s [-(1 - \alpha)p_- + \alpha p_+] = 2Q_{33}^f P_s (2\alpha - 1)\chi_f E, \tag{3.14}$$

Table 2: Extrinsic Dielectric Constants of PZT and BaTiO₃
 (Divided by permittivity of vacuum $\kappa_0 = 8.85E-12$)

	PT	PZT 20/80	PZT 40/60	PZT 50/50	BT
K_{DI}	114	140	147	125	77.1
K_I	204	270	290	182	63.8
K	258	290	300	401	87.8

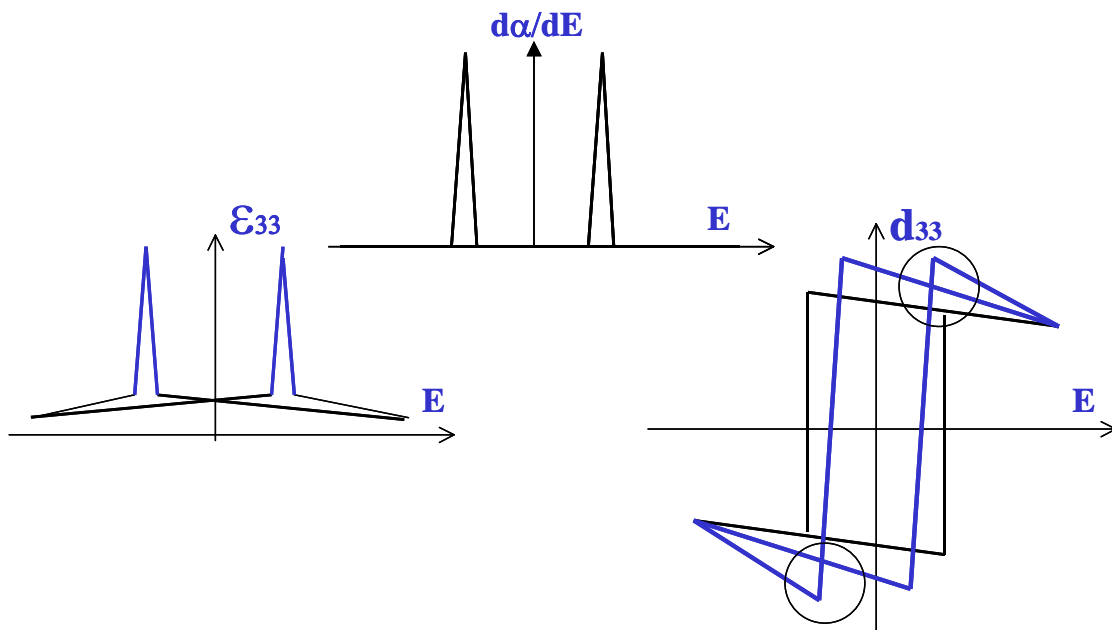


Figure 3.3: Dependence of polarization, piezoelectric and dielectric constants on the applied electric field for a film consisted of 180° ferroelectric domains, including extrinsic effects due to domain wall movement. The two peaks at the left bottom are corresponding to the extrinsic contribution in dielectric measurement. The circled areas in the right bottom are “noses” of piezoelectric hysteresis loop, which is corresponding, to the extrinsic contribution.

$$\text{where } Q_{33}^f = Q_{33} - \frac{2S_{13}}{S_{11} + S_{12}} Q_{31}. \quad (3.15)$$

Therefore the effective piezoelectric modulus is

$$d_{33}^{eff} = \frac{d\varepsilon_{eff}}{dE} = [(2\alpha - 1) + 2E \frac{d\alpha}{dE}] d_{33}^f, \quad (3.16)$$

where

$$d_{33}^f = 2Q_{33}^f P_s \chi_f \quad (3.17)$$

is the piezoelectric modulus of a clamped single domain film. The first term in the right hand of Eq. (3.16) is the intrinsic contribution to piezoresponse due to domain fraction. The second term in the right hand of Eq. (3.16) is the extrinsic contribution to piezoresponse due to the domain fraction changes under electric field. In the piezoelectric force microscopy measurements, the extrinsic contribution is large near the coercive field and leads to the tip position in the “nose” of various butterfly loops (Figure 3.3).

3.3 Discussion of dielectric and piezoelectric hysteresis loops

Eq. (3.13) and Eq. (3.16) describe the effective dielectric and piezoelectric response of 180° ferroelectric domains, which not only depends on materials constants, but also depends on the domain fraction and its relation with electric field: $\alpha(E)$. The function $\alpha(E)$ cannot be determined in a thermodynamic approach, because the change of domain volume fraction versus electric field depends on sample history, internal structures and the external field pulse length and frequency. For simplicity we may assume an ideal equilibrium process from $\alpha=0$ (unswitched) to

$\alpha=1/2$ (half switched) and finally $\alpha=1$ (complete switched) under a slowly increasing switching electric field. When $\alpha=0$ (unswitched), $d\alpha/dE$ is close to 0, so $\chi_{eff} = \chi_f$, $d_{33}^{eff} = -d_{33}^f$; similarly when $\alpha=1$ (completed switched), $d\alpha/dE$ is also close to 0, thus $\chi_{eff} = \chi_f$, $d_{33}^{eff} = +d_{33}^f$. But when $\alpha=1/2$ (half switched), the electric field is coercive field E_c and the dielectric constant measurement should give

$$\chi_{eff}^{E_c} = 2 \left(\frac{d\alpha}{dE} \right)_{E_c} P_s + \frac{\chi_f k}{\chi_f + k}, \quad (3.18)$$

and the piezoelectric measurement comes out with an effective value

$$d_{33}^{E_c} = 2E_c \left(\frac{d\alpha}{dE} \right)_{E_c} d_{33}^f, \quad (3.19)$$

which is the tip position in the hysteresis loops (Figure 3.2). In fact the effective piezoelectric constant should be close to zero at a field smaller than E_c according to Eq. (3.15), which also predicts a smaller estimated coercive field E_c from a piezoelectric hysteresis loop measurement than that from dielectric measurement or polarization hysteresis characterization. This conclusion means that the apparent coercive field that is determined from piezoelectric hysteresis is questionable even though it is widely used in thin film characterizations.

In a high-frequency measurement, it is possible to consider the domain structure unchanged. If we neglect the $\alpha(E)$ derivative dependence, Eq. (3.13) and Eq. (3.16) can be simplified into intrinsic terms as

$$\chi_{eff} = \frac{\chi_f [k + (2\alpha - 1)^2 \chi_f]}{\chi_f + k}, \quad (3.20)$$

$$d_{33}^{eff} = (2\alpha - 1)d_{33}^f$$

which may provide a path to get $\alpha(E)$ dependence. However, in the experiments of ferroelectric or piezoelectric characterization including the hysteresis measurements of polarization, dielectric and piezoelectric properties, frequency dependence always exists. Even in a “quasi-static” d_{33} - E loops measured by a lock-in technique, small ac signals are applied to the AFM tip to get the displacements of a film surface. The ac signals, if not small, can drive the movement of 180° domain walls, so it’s not reasonable to assume current d_{33} - E measurement set-up using AFM can provide unquestionable intrinsic effective d_{33} results if the film is not always a single domain film. Therefore, we have to take into account the $\alpha(E)$ derivative dependence driven by ac field.

A simple explanation for the shape of the piezoelectric hysteresis loops piezoelectric coefficient d vs. applied electric field E including ac $\alpha(E)$ derivative dependence can be developed for the case of 180° domain switching in ferroelectrics. The average of the ac *derivative* of $\alpha(E)$ is

$$\left(\frac{d\alpha}{dE}\right)_{ac} \cong \frac{\alpha(E_{dc} + E_{ac}) - \alpha(E_{dc} - E_{ac})}{2E_{ac}}, \quad (3. 21)$$

where E_{ac} is the ac field amplitude. We can estimate the extrinsic contribution driven by ac field from domain walls motion (domain fraction change). Because of the hysteretic nature of the function $\alpha(E)$, in general, the ac derivative differs from the corresponding normal derivative of $P(E)$, just like the C-V curve of a ferroelectric capacitor is in general different from the field derivative of its polarization loop.⁴⁴ Eq. (3. 21) takes an approximation of d_{33} measurement by averaging the $\alpha(E)$ dependence. By assuming a slow process of applying electric field with enough long

time to wait it close to equilibrium, we get $\alpha-E$ dependence from $P-E$ dependence in a first order approximation.

The illustrations of the relationships of $P-E$, $\alpha-E$, $\chi-E$, $d_{33}-E$ have been shown in Figure 3.3. We know that even for a single domain film, on the contrary to the common linear behavior, $d_{33}-E$ curve is not simply repeating the curve of $P-E$, it should include the dependences of both $P-E$ and $\chi-E$.²⁷

In Figures 3.4 and 3.5, we show an example of experimental measurements for a 50 nm PZT 20/80 thin film. The dramatic change of $\alpha(E)$ happens close to E_c , which gives additional contribution to $\chi-E$, $d_{33}-E$ measurements. According to Eqs.(3. 16) and (3. 21), this extrinsic contribution to piezoreponse is estimated to be 1.12 times as large as the intrinsic piezoresponse of a single domain film under 2V peak-to-peak ac field. In chapter 2, the electric field dependence of single domain film already predicts the largest value occurs at a negative field, but it cannot explain the butterfly loops. This additional increase at the tip position compared with that of a single domain film in the piezoelectric loop is 12%. It can become much larger in the cutting thin film islands or under larger ac field. The apparent E_c determined from piezoelectric hysteresis loop is much less than the one determined from polarization hysteresis loop.

There may exist many different kinds of ferroelectric hysteresis loops depending on film quality, back switching fractions and pinning status.⁴⁴ We present the results for a single crystalline film consists of only 180 degree domains and this result can only be used in such assumptions. For films with other polydomain structures, for

example, a relatively thicker film consisting of 90-degree polydomain, the extrinsic effects due to 90-degree domain walls movement can be treated in a similar manner.

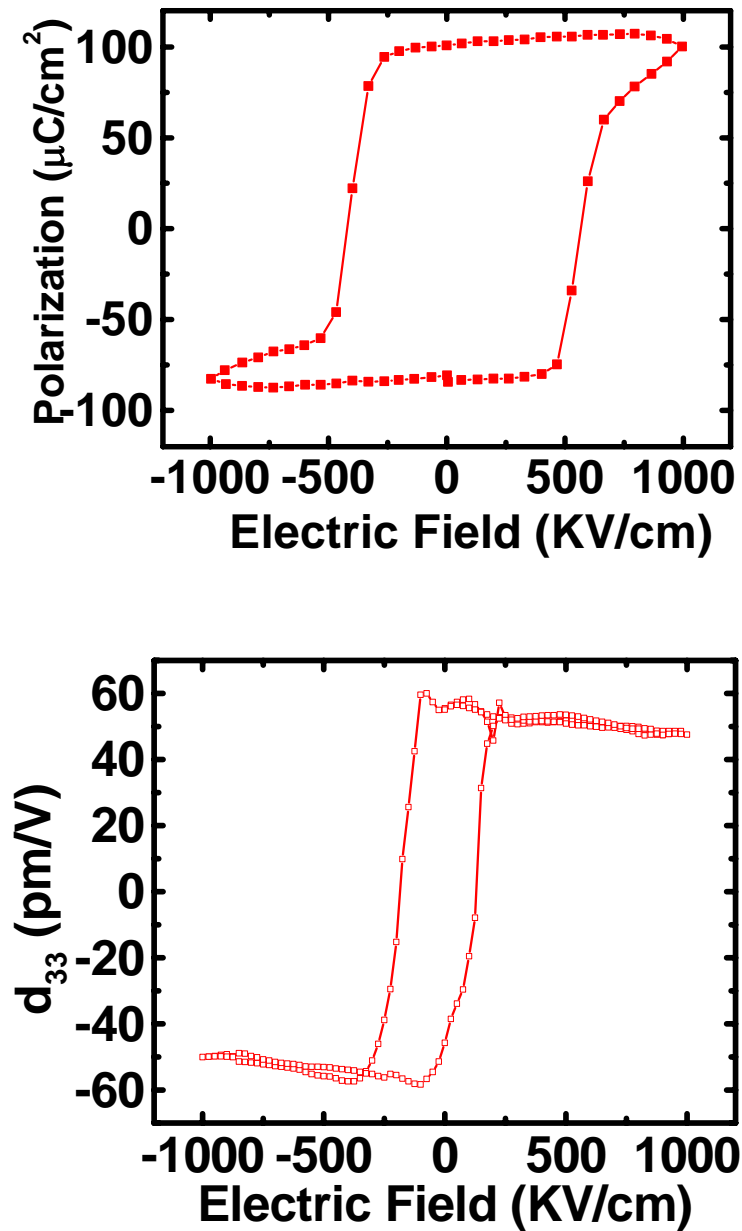


Figure 3.4: Experiment measurements of a 50 nm PZT 20/80 film.

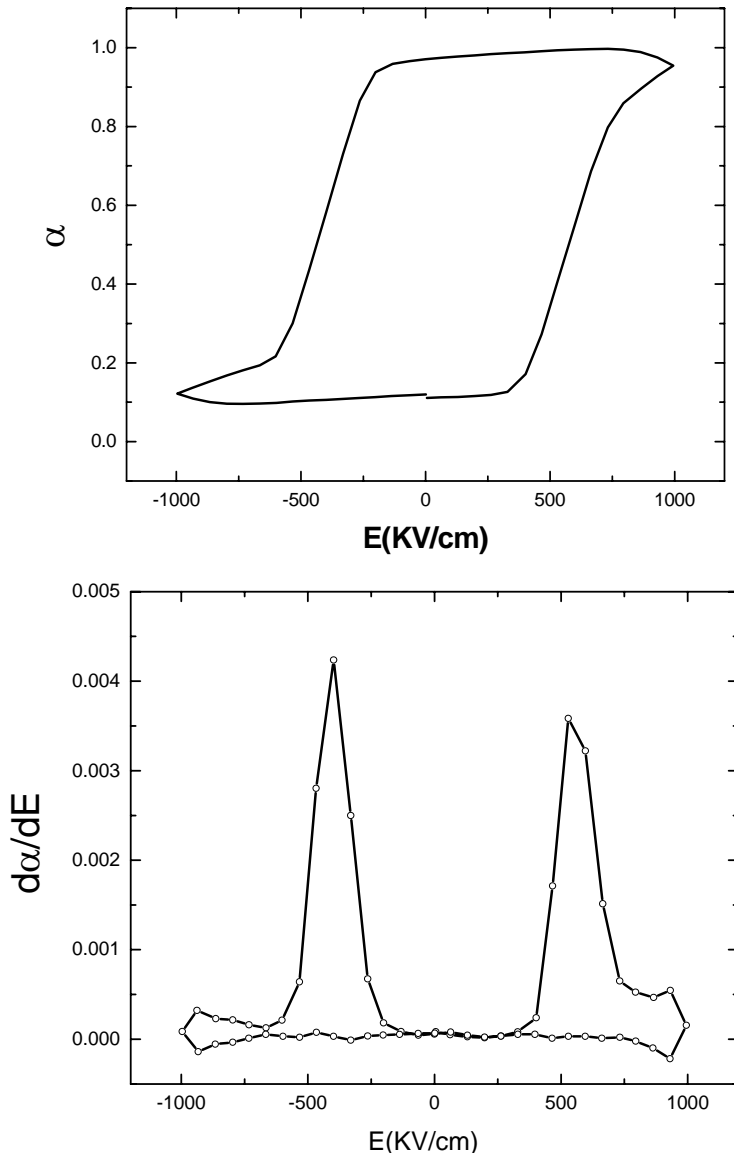


Figure 3.5: Analysis of the extrinsic effects in a 50 nm PZT 20/80 thin film.

3.4 Effects of elastic interactions on switching in thin films

The competition between electric energy and elastic energy in Eq. (3.6) may lead to some interesting questions: (1) the switching may not be stable under large antiparallel electric field. It is likely to happen in very thin films with large electric field and large piezostress. The driving force for a new 180° domain to form (switching happens) is $-2PsE$, while the elastic interaction barrier for it to form under large electric field is $(e^{DI}-e^I)$, it increases proportional to the square of electric field when the field strength is larger than a critical field $E_{cr} \sim (2-3) \times 10^8$ V/m, the free energy change is positive and the switching is unstable. (2) As $e^{DI} > e^I$, the energy increased by direct interaction between domains is larger than the energy released by indirect interaction between domains throughout the substrate. It is expected that, the electrostatic energy decrease will dominate at low field, and domain switching will take place. While at some level of high field, the elastic energy increases proportional to the square of electric field, resulting in a minimum total energy at a certain domain fraction hence inhibit the complete switching of the film. The stability condition of α requires that $\frac{\xi^* D}{h} > \frac{e^{DI}}{e^I} - 1$ to make $\frac{\partial^2 F}{\partial^2 \alpha} > 0$, which means the striped-domain period D is close to the thickness of film h . This can only happen in ultra thin film with wide 180° domains.

As discussed in next chapter, local writing experiments have already presented experimental proofs⁴⁵ for the existence of large piezostress due to the 180° domain interaction after a local switching, where the large piezostress between 180° domains can be released by the formation of 90° elastic domains.

On the other hand, the polarization switching in single-crystalline ferroelectric films has been investigated experimentally and theoretically because of its importance in the application of memory devices. For example, the hysteresis loops were measured for PZT 20/80 films with thickness ranging from 8 to 100 nm.⁶⁰ These films were grown epitaxially on SrRuO₃ bottom electrodes deposited on SrTiO₃ substrates. The measurements using SrRuO₃ top electrodes showed that the coercive field E_c increases dramatically as the film becomes thinner, reaching values as high as $E_c=1000$ kV/cm and reaches the thermodynamic coercive field E_{th} of a ferroelectric film in an epitaxial system.^{61,62}

The intrinsic thermodynamic coercive field for a single domain film can be calculated by considering the minimum polarization that can exist in an antiparallel electric field E_{th} . The stability condition for Eq.(2.20) $E = \alpha P + \beta P^3 + \alpha_3 P^5$

is $\frac{\partial E}{\partial P} = \alpha + 3\beta P^2 + 5\alpha_3 P^4 = 0$. The critical polarization can exist in E_{th}

obeys $P_c^2 = \frac{-3\beta + \sqrt{9\beta^2 - 20\alpha\alpha_3}}{10\alpha_3}$, so $E_{th} = \alpha P_c + \beta P_c^3 + \alpha_3 P_c^5$ can be simplified

as $E_{th} = -2\beta P_c^2 - 4\alpha_3 P_c^4$, which has been calculated and listed in Table 2 for zero misfit.

A possible explanation for the coercive field in thin film approaches the thermodynamic coercive field is that, the large electric field make the nucleation and growth of 180 degree domains in thin films much difficult due to the strong elastic interactions between 180 degree domains. Therefore the switching of relatively thin film is due to the thermodynamic instability instead of the process of 180° domain

nucleus forms and expands. Most of the previous discussions about interdomain elastic interactions are based on a dense domain model ($D \ll h$). More complexity exists in calculating the inhomogeneous elastic interactions for the case $D \sim h$ or $D > h$, which is possible in a thinner film and ultra thin film. The full understanding of the elastic interaction within the domains of all possible configurations may shed light to explain the thickness dependences^{60,63} of many ferroelectric and piezoelectric properties.

Table 3: Thermodynamic coercive fields for bulk and thin films (misfit=0)

	Ec, bulk (V/m)	Ec, film (V/m)
PTO	1.590E+08	2.851E+08
PZT 20/80	1.181E+08	1.943E+08
PZT 40/60	4.666E+07	8.193E+07
PZT 50/50	2.235E+07	5.608E+07

3.5 Conclusion

The elastic interactions between 180° ferroelectric domains under an external electric field has been introduced and explained. The effects on the dielectric and piezoelectric response of 180° ferroelectric thin films including intrinsic and extrinsic contributions are calculated and presented. The extrinsic contributions are notable and can be used to explain the characteristics in dielectric and piezoelectric hysteresis loops are explained for a thin film consisted of 180° ferroelectric domains. These elastic interactions are also important on the stabilities of switching in thin films.

Chapter 4: Formation of 90° elastic domains during a local 180° switching in epitaxial ferroelectric thin films

4.1 Introduction

Nanoscale visualization and control of ferroelectric domains with piezoresponse microscopy (PFM) have been reported intensively.⁶⁴⁻⁶⁹ Controlled ferroelectric domain structures may be engineered by applying a voltage between an atomic force microscopy (AFM) tip and a bottom electrode of a ferroelectric thin film.⁶⁵ The reversal of polarization by 180° in tetragonal ferroelectric materials such as PZT has been conventionally thought to be stress-free. The c^+ and c^- domain are elastically identical without electric field. But under electric field, due to the opposite signs of the converse piezoelectric effects in c^- domain and c^+ domains, one domain elongates while the other shrinks as shown in Figure 3. 1. Due to the mechanical compatibility of the domains, the differences of strains in the domains are sources of internal stress. This inter domain clamping effect is especially important for ferroelectric thin film under large electric field, as we already discussed in chapter 3. In this chapter, we demonstrate that a cylindrical 180° domain can be stabilized by the formation of 90° domains to relax stress due to the opposite signs of the converse piezoelectric strains inside the switched 180° domain and the unswitched film.⁴⁵ In the local switching experiment, large local field and corresponding piezostress are created under the AFM tip. The local electric field under the AFM tip creates a 180° domain and induces piezostress due to the opposite signs of piezostress inside and outside of the

domain as shown in Figure 4.1(a) and (b). The stress relaxes by the formation of 90° domains or twinning in this 180° domain illustrated in Figure 4.1(c). The 90° domains, serving as elastic domains, decrease the piezostress of the 180° domain and therefore the elastic energy of the piezostress. This is a thermodynamic reason of the jointed formation of a 180° domain and 90° domains. After the electric field is turned off, 90° domains should expand through the film and form a stable configuration with the 180° domain shown in Figure 4.1(d).

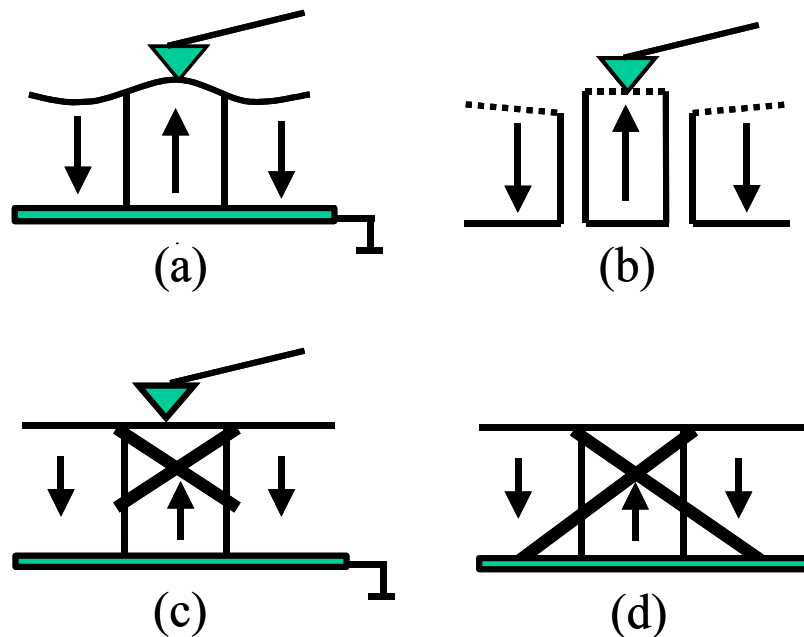


Figure 4.1: (a) A reversed 180° domain under an AFM tip, (b) Piezostress of the 180° domain under electric field, (c) Relaxation of piezostress through formation of new 90° domains. (d) After the field is turned off, 90° domains expand through the film and form a stable configuration.

4.2 Experiment observations

A heterostructure with epitaxial (001) PZT 20/80 thin films of varying thickness were deposited onto single-crystal (001) SrTiO₃ substrates (Crystec GmbH, Germany) or onto a buffer layer of SrTiO₃ on Si substrates by pulsed laser deposition (PLD) at 650°C and 100 mTorr oxygen partial pressure. The samples were cooled at a rate of 1 °C/min from the growth temperature. The thicknesses of the films were confirmed by Rutherford backscattering and TEM. Conducting perovskite La_{0.5}Sr_{0.5}CoO₃ (LSCO) or SrRuO₃ (SRO) electrodes were used as bottom and top electrodes, also deposited by PLD.^{60,66}

Domain structures have been observed by PFM (Figure 4.2) and by x-ray diffraction. The ferroelectric heterostructure used in this study consisted of 50-400 nm thick PZT films epitaxially grown on a (001) single crystalline SrTiO₃ (STO) substrate with an intermediate 50 nm-thick La_{0.5}Sr_{0.5}CoO₃ (LSCO) oxide layer employed as the bottom electrode. At room temperature, as-grown PZT films with thickness larger than 200 nm displayed the presence of a two-dimensional grid of 90° domains embedded into the ferroelectric matrix with the tetragonal *c* axis being oriented orthogonal to the substrate. Nanoscale visualization of the film domain structure shown in Figures 4.2 and 4.3 was carried out with the aid of a commercial Digital Instruments Nanoscope IIIA Multimode scanning probe microscopy. The typical force constant of the tips is 5 N/m and the apex radius is approximately 5-15 nm. This technique enabled us to differentiate between the *c* and *a* domains and to determine their polarization directions. Investigation of the as-grown film showed that the out-of-plane polarization in *c* domains points preferentially towards the

bottom electrode, namely c^- domain. This can be seen as the region with light contrast and could be attributed to the absence of a top electrode and the subsequent development of internal built in electric field. θ - 2θ scans using a Siemens D5000 4-circle x-ray diffractometer with monochromatic Cu K α radiation revealed the presence of c -axis domains (with polarization normal to the film), 90° -domains (with polarization in the plane of the film) and the absence of any secondary phases. The 90° -domain volume fraction was calculated from the θ - and ω -rocking curves. The 100 nm film has no discernible 90° -domains; films thicker than 150 nm relax the transformation strain through the formation of a 2-dimensional array of 90° -domains. Quantitative x-ray diffraction measurements yield a 90° -domain fraction of about 30% for a 300 nm thick film, which increases to about 50% at a thickness of 1 μm .

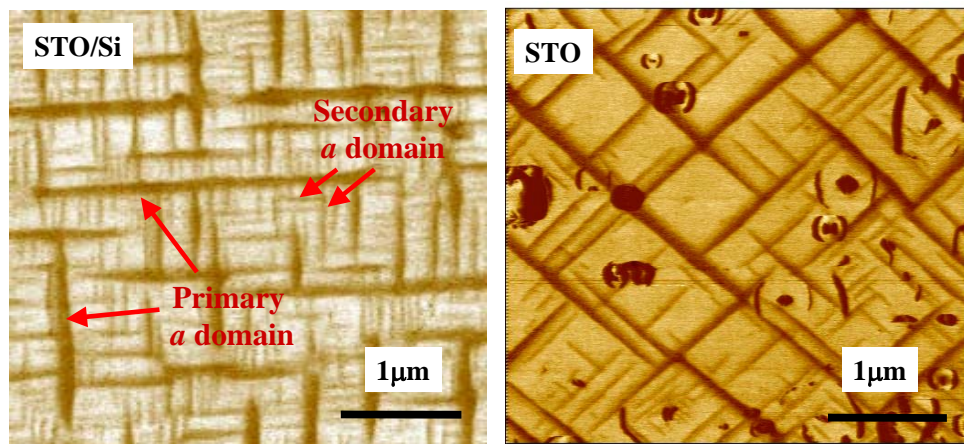


Figure 4.2: Piezoresponse microscopy measurements of domain images for 1 μm thick PZT 20/80 films deposited on STO/Si and STO substrates.

Using the PFM method, the formation of new 90° domains has been observed after localized poling of c^- domains in the 400 nm- thick epitaxial $\text{PbZr}_{0.2}\text{Ti}_{0.8}\text{O}_3$ (PZT 20/80) thin films. The AFM tip was then placed at the position marked by a '+' and dc pulse of -12V was applied to the tip for one second with the bottom electrode grounded as show in Figure 4.3 (b). A subsequent piezoresponse scan of the same region of the film clearly shows a reversed c^+ domain, which is noticed by the dark contrast in Figure 4.3 (c), and newly formed a domains in Figure 4.3 (d) and (e). These 90° domains were seen to form independent of the mechanical pressure applied with the AFM tip within the experimental range of applied contacted forces and could not be formed without a negative poling electrical pulse against polarization, so the formation of 90° domain cannot be a result of the mechanical compress stress created by tip's contact force, although it is claimed to be possible in Ref. 67. On the other hand, no new elastic domains were observed under positive poling along the direction of the polarization of as-grown c^- films as shown in Figure 4. 4. All these experiment facts can be explained on the basis of the idea that formation of new 90° domain is a mechanism of relaxation of piezostress created by the 180° domain structure in the electric field of the tip.

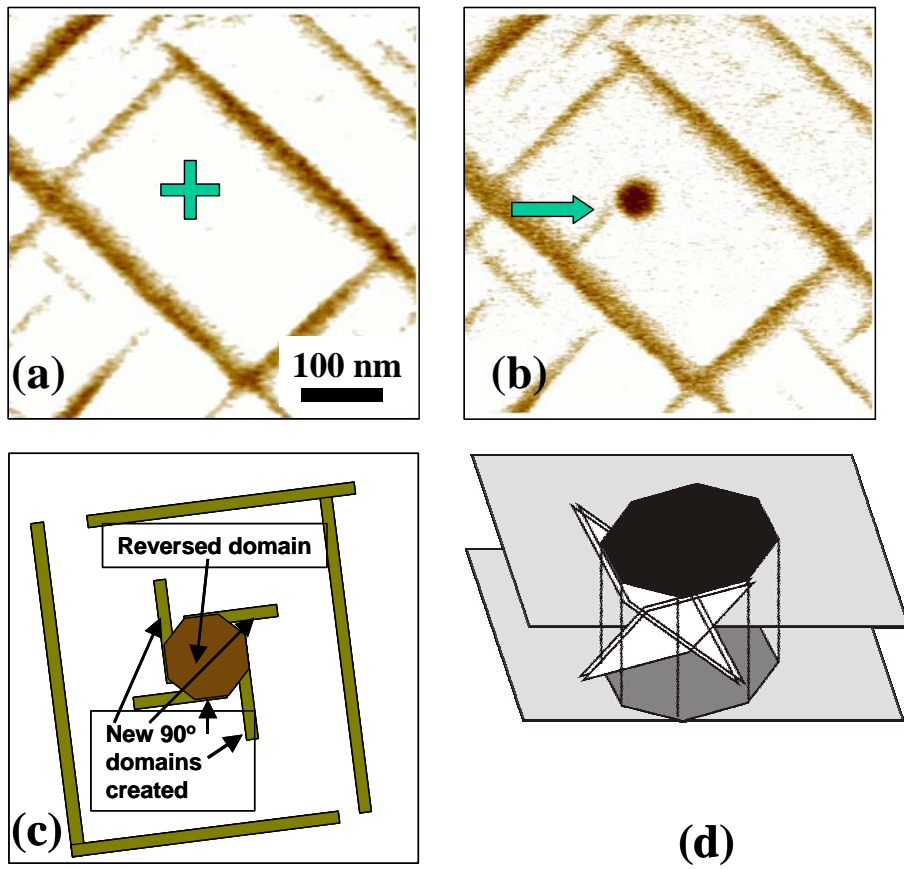


Figure 4.3: (a) PFM domain structure image, (b) PFM image after a local switching with a -12V pulse for one second at site marked with '+' in (b), (c) Plan view diagram of new 90° domains formed and reversed 180° domain, (d) 3-D view diagram of new 90° domains formed and reversed 180° domain.

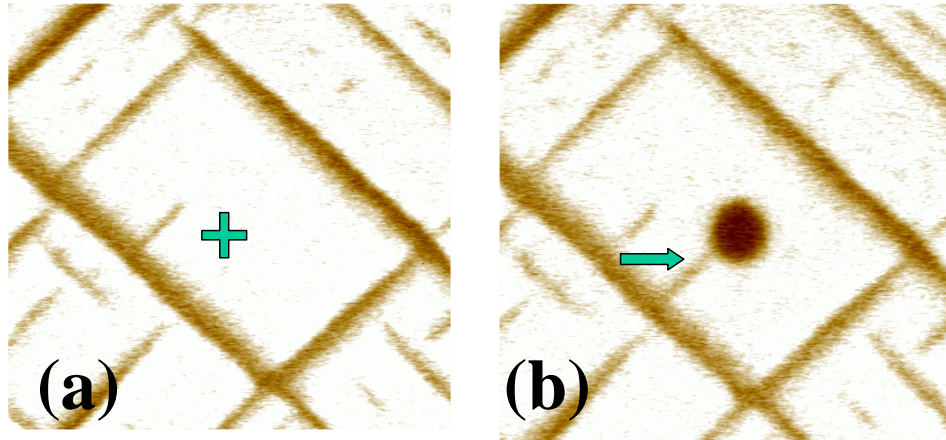


Figure 4.4: (a) PFM image after a positive local switching with a +12V pulse for one second at site marked with '+', no new 90° domains were formed. (b) New 90° domain was formed near the same site marked with '+' with a reversed 180° domain.

4.3 Thermodynamic estimations

The formation of elastic domains is a universal mechanism of relaxation of internal stresses in constrained phase transformation in solids.⁷²⁻⁷⁵ The arrangement of elastic domains determines most of the physical properties of the product phase. Most of previous studies considering elastic domain structure in epitaxial films were concentrated on elastic domain assemblies consisting of two types of domains (polytwins).⁷⁶⁻⁷⁸ The two-domain structures are able to relax misfit stress only partially, reducing biaxial stress to a uniaxial one. The complete relaxation, in general, requires the formation of polydomain structures including more than two types of possible domains.⁷⁸⁻⁷⁹ The three-domain structures are thermodynamically more preferable than two-domain ones provided films are not very thin (Figure 4.5).

The three-domain structures have been observed recently in ferroelectric tetragonal $\text{PbZr}_{0.2}\text{Ti}_{0.8}\text{O}_3$ (PZT 20/80) films with thickness more than 200 nm and it has been shown that the misfit stress in these films is close to zero.⁷⁹⁻⁸³

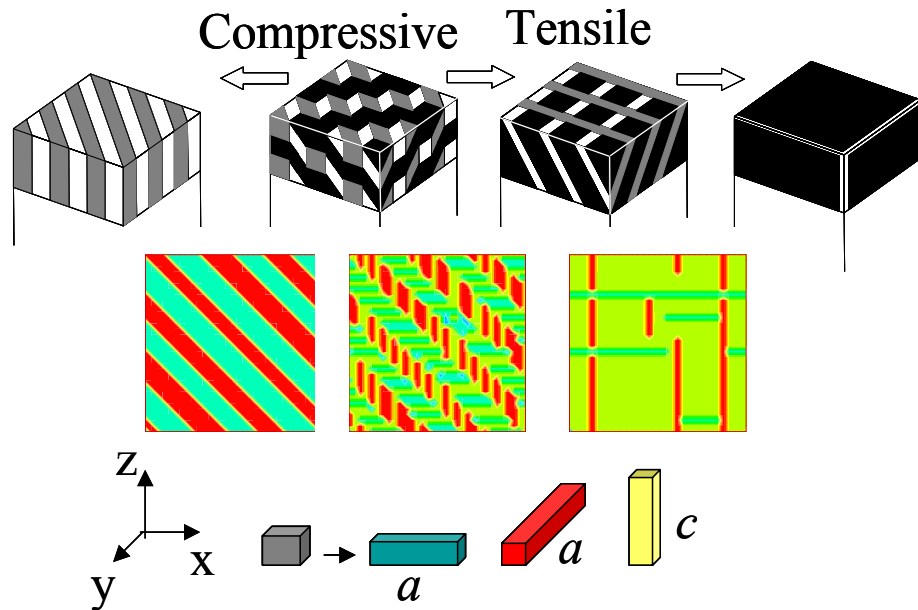


Figure 4.5: 3-dimensional polydomain structures in epitaxial films. Figure adapted from Ref. 80.

To make the linear description of polydomain films mathematically feasible, it is necessary to assume the polarization and strain fields to be homogeneous within each domain. This approximation may be justified for dense laminar polydomain states,⁵² where the domain widths are much smaller than the film thickness. Such domain structures become energetically most favorable in epitaxial films with a thickness larger than about 200 nm.

The transformation from cubic paraelectric phase to tetragonal ferroelectric phase, is accompanied by a self-strain that can be characterized for a_1 , a_2 , and c domains, respectively as shown in Figure 4.5 with the self-strain tensors

$$\hat{\varepsilon}_1 = \begin{pmatrix} \varepsilon_c & 0 & 0 \\ 0 & \varepsilon_a & 0 \\ 0 & 0 & \varepsilon_a \end{pmatrix}, \hat{\varepsilon}_2 = \begin{pmatrix} \varepsilon_a & 0 & 0 \\ 0 & \varepsilon_c & 0 \\ 0 & 0 & \varepsilon_a \end{pmatrix}, \hat{\varepsilon}_3 = \begin{pmatrix} \varepsilon_a & 0 & 0 \\ 0 & \varepsilon_a & 0 \\ 0 & 0 & \varepsilon_c \end{pmatrix}, \quad (4.1)$$

where

$$\begin{aligned} \varepsilon_a &= Q_{31}P^2, \varepsilon_c = Q_{33}P^2 \\ d_{31} &= 2PQ_{31}\chi_{33}, d_{33} = 2PQ_{33}\chi_{33} \end{aligned} \quad (4.2)$$

In Eq.(4.2), Q_{31} and Q_{33} are the electrostrictive coefficients in the Voigt notation, P is the polarization, χ_{33} is the dielectric susceptibility, and d_{31} and d_{33} are the piezomoduli of an unstressed single domain ferroelectric film (or bulk). The data for these parameters are already given in previous chapters.

The simple thermodynamic analysis allows us to outline necessary conditions for piezostress relaxation through the elastic domain formation.⁴⁵ For simplicity, we may assume that the electrostatic field under the tip concentrated in the switched domain can be characterized by an average E . Then the elastic stress in the domain is $\sigma = G(dE)$, where dE is the piezostress, d is the piezomodulus and G is the effective elastic modulus, depending on elastic properties of film and substrate and the geometry of the system, particularly on the shape of the domain

The elastic stress decreases if the elastic strain decreases, resulting from the formation of twins with: 1) spontaneous strain $\varepsilon_0 = \varepsilon_c - \varepsilon_a$, where ε_c and ε_a are self-strain of a - and c - domains in Eqs. (4.1) and (4.2); 2) the difference of electric field

induced piezostain between them, ΔdE . Thus the free energy change due to the formation of elastic domains inside a 180° domain under electric field E is

$$F(\alpha, E) = (1/2)G\{[dE - \alpha(\varepsilon_0 + \Delta dE)]^2 - (dE)^2\} + \alpha[(1/2)(\chi_a - \chi_c)E^2 + PE] + \sigma_M[dE - (\alpha\varepsilon_0 + \Delta dE)] \quad (4.3)$$

where α is a volume fraction of twins (90° elastic domains), P is the saturation polarization and σ_M is misfit stress. The first term in the right hand of Eq. (4.3) is the elastic energy decrease after the formation of the twinned domain, $dE - \alpha(\varepsilon_0 + \Delta dE)$ is the elastic strain due to the formation of 90° domains, the second one expresses electrostatic energy increase due to the formation of 90° domains and the last one is the effect of misfit stress of the film. Misfit effect in thin film can be very important but it is not considered here by assuming nearly complete release of misfit stress by forming 90° domain grids in the as-grown films after annealing, and will be omitted hereafter.

Assuming cylindrical shape of the reversed domain, the isotropic elastic energy per unit volume of the domain is

$$e = [Y/2(1 - \nu^2)][(\varepsilon_{xx} + \nu\varepsilon_{zz})^2 + (1 - \nu^2)\varepsilon_{zz}^2] \quad (4.4)$$

where Y is Young's modulus, ν is the Poisson ratio, and the principal strains after formation of new elastic domains are

$$\begin{aligned} \varepsilon_{xx} = \varepsilon_{yy} &= d_{31}E + (1/2)\alpha[\varepsilon_0 + (d_{33} - d_{31})E] \\ \varepsilon_{zz} &= d_{33}E - \alpha[\varepsilon_0 + (d_{33} - d_{31})E] \end{aligned} \quad (4.5)$$

and before the formation of new elastic domains:

$$\begin{aligned} \varepsilon_{xx}^0 = \varepsilon_{yy}^0 &= d_{31}E \\ \varepsilon_{zz}^0 &= d_{33}E \end{aligned} \quad (4.6)$$

Omitting misfit contributions, Eq. (4.3) can be rewritten as:

$$F(\alpha, E) = [Y/2(1-\nu^2)][(5-4\nu)\varepsilon_1^2 + (2d_{31} - 4d_{33} - 4\nu d_{31} + 2\nu d_{33})E\varepsilon_1] + \alpha[(1/2)(\chi_a - \chi_c)E^2] + PE, \quad (4.7)$$

where $\varepsilon_1 = \frac{1}{2}\alpha[\varepsilon_0 + (d_{33} - d_{31})E]$, χ_a and χ_c are the susceptibilities of *a*- and *c*-

domain under electric field. The relaxation of piezostress by twinning is possible and

stable only if $\alpha > 0$ and $d^2F/d\alpha^2 > 0$. If we set $\gamma = -d_{31}/d_{33}$, minimum of free

energy in Eq. (4.3) gives

$$\alpha_0 = \frac{(2\gamma + 4 - 4\nu\gamma - 2\nu)d_{33}E}{(5 - 4\nu)[\varepsilon_0 + (1 + \gamma)d_{33}E]} - \frac{4(1 - \nu^2)[(1/2)(\chi_a - \chi_c)E^2 + PE]}{Y(5 - 4\nu)[\varepsilon_0 + (1 + \gamma)d_{33}E]^2}. \quad (4.8)$$

In order to make $\alpha_0 > 0$, Eq. (4.8) gives

$$C[d_{33}\varepsilon_0 + (1 + \gamma)d_{33}^2E] > (\chi_a - \chi_c)E/2 + P, \quad (4.9)$$

where $C = \frac{Y(\gamma + 2 - 2\nu\gamma - \nu)}{2(1 - \nu^2)}$ is the effective modulus. This criterion given by Eq.

(4.9) means the relief of the elastic energy exceeds the increase of the electrostatic

energy. The formations of 90° domains in the electric field under the tip proceeds

against this field because it decreases the average net polarization along this field,

therefore the piezoelectric stress should be significantly large to make the trend

towards stress relaxation to overcome the electric field which opposes to the

formation of 90° domain, which plays here as an elastic domain. The sign of Eq. (4.9)

only depends on materials intrinsic properties and field *E*. It can be easily understood

that ferroelectric materials with large d_{33} , large spontaneous strain ε_0 and small

difference between the susceptibilities of *a* and *c* domain can fulfill this requirement

Taking standard ferroelectric lead titanate (PT) and barium titanate (BT) single

crystals for example: in simple estimation, both γ and ν almost equal to 1/3, so C nearly equals to Y , which is 160 GPa for PT and 200 GPa for BT; d_{33} of PT is 80, BT 132 pm/V; spontaneous strain ε_0 of PT is 6.5%, BT 1.1%; spontaneous polarization of PT is 0.75, BT 0.26 C/m²; the difference between dielectric constants in-plane and out-of-plane for PT is 60, for BT is as large as 2000~3000. In a field E large than 3.4×10^5 V/m, BT cannot fulfill this requirement while PT always can. The data used for calculations are listed in Table 4.

Since the electric field under AFM tip can be even larger than this value, we don't expect this relaxation mechanism can occur in BT samples. We have to admit this is a simplified estimation based on single crystal values, while the thin films should have less d_{33} and polarization compared to single crystal due to substrate clamping. Using this criterion of Eq. (4.9), the relaxation mechanism still works for PT and PZT 20/80 thin films.

Table 4: Estimation of necessary condition of relaxation of piezostress through new elastic domain formation

	γ	ε_0	d_{33}	$\chi_a - \chi_c$	P_s	E (limit)
BaTiO3	1/3	1.1%	132	2500	0.26	Cannot
PbTiO3	1/3	6.5%	79.2	57.4	0.75	>3.6e6
PZT 20/80	1/3	5.2%	87.2	56.6	0.70	>4.5e6
PZT 50/50	1/2	3.6%	327	1339	0.50	Cannot

In the PFM experiments on PZT 20/80 thin films, the electric field distribution under the tip is highly inhomogeneous.⁶⁶⁻⁷¹ The field strength is the largest just beneath the tip and almost proportional to the inverse of distance from the tip. It's reasonable to expect the piezoelectric stress distribution therein could also be very inhomogeneous. Therefore the elastic domain densities also follows inhomogeneous distribution which suggests relatively much larger elastic domain fraction in the top surface area close to the tip than those far away from it. In this 400 nm thick PZT 20/80 film, the applied voltage is -12V, the contact potential difference between the conductive tip and sample typically does not exceed 2V, the dielectric constants in-plane and out-of-plane are 143 and 86.4 respectively, tip radius is 5~15 nm, we take 10 nm. If the attenuating factor γ of the surface potential compared with tip potential is not very small i.e. in a contact strong indentation limit:⁶⁹ $\gamma = (1 + wk_{eff} / ak_d)^{-1}$, where w is the thickness of the “apparent dielectric gap” for doped silicon tip, we take $w=0.1$ nm; a is the radius of tip, 10 nm; and take $k_{eff}=100$ for PZT 20/80 and $k_d=7$ for apparent dielectric gap; we get the attenuating factor $\gamma = 7/8$. The calculated field near the top surface under the tip is close to 6×10^8 V/m, following Eq. (4.8), it gives about 17% of elastic domain fraction; while in the bottom surface of the film, electric field is only 1.1×10^6 V/m, coming with almost negligible piezostress and therefore elastic domain fraction is close to zero.

4.4 Conclusion

We can get two important conclusions from this study: 1) the elastic energy of piezostress is a considerable contribution in the thermodynamics of switching domain under electric field, particularly for thin films under large electric field; 2) the relaxation of piezostress is essential even if it is not a controlling factor in the switching of 180° domains in thin films. The analysis of numerical values included in the criterion of twinning relaxation (Eq. (4.9)) shows that this condition is satisfied marginally, i.e. ferroelectric materials with special relation between the electrical and mechanical parameters are available for such a kind of relaxation. Therefore the further investigations of twinning relaxation as well as other mechanism of stress relaxation become a necessary step for the full understanding of the polarization switching in ferroelectric films. This chapter also served as an experimental proof of the elastic interactions between 180° domains in thin films as discussed in chapter 3.

Chapter 5: Contribution of substrate to converse piezoelectric response of constrained thin films

5. 1: Introduction

Understanding of the piezoresponse of piezoelectric thin films is essential in the design and fabrication of micro sensors, actuators and other electromechanical devices.⁸⁴⁻⁸⁹ In principle the converse piezoresponse, may be characterized by applying a voltage (field) and measuring the field-induced strain. For example, if a thin film has a tetragonal structure with the polarization along c axis normal to the film (along z direction), and epitaxially oriented on a cubic substrate layer with the interface along $(001)_T // (001)_C$, the field-induced strain in the film is:

$$\hat{\varepsilon}_0 = \begin{bmatrix} d_{31}E & 0 & 0 \\ 0 & d_{31}E & 0 \\ 0 & 0 & d_{33}E \end{bmatrix}, \quad (5.1)$$

where d_{33} , d_{31} are the longitudinal and transverse piezoelectric coefficients of a free-standing piezoelectric film, and E is the applied electric field normal to the film. From the calculation of the total strain in the film clamped by a substrate, it has been concluded that the effective piezoelectric coefficient of the thin film follows³¹

$$d_{33}^f = d_{33} - \frac{2d_{31}S_{13}^f}{(S_{11}^f + S_{12}^f)}, \quad (5.2)$$

where S_{ij}^f are the mechanical compliances of the film under constant electric field. Eq.

(5. 2) demonstrates that d_{33}^f measured by the strain in the film is independent of elastic properties of a substrate if the film is completely clamped by the substrate.

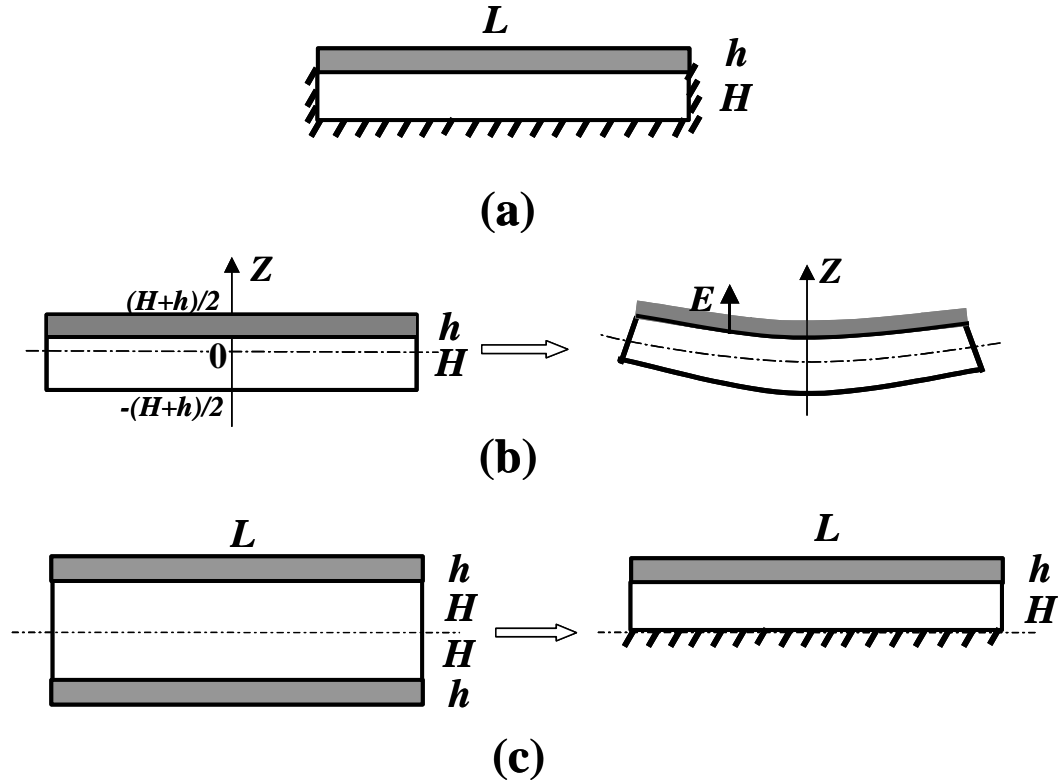


Figure 5. 1: Different boundary conditions of a thin film (h) on a much thicker substrate (H): (a) Fixed bottom and side surfaces of the substrate; (b) Bending of two-layer plates consisting of a piezoelectric thin film and a substrate, initial state of the film and substrate (left) and the thin film and substrate under the electric field along z coordinates (right); (c) A symmetrical three-layer film/substrate/film stack (left), corresponding to the fixed bottom surface of the substrate (right).

However, the piezostain of a constrained thin film cannot be directly measured by the standard resonance method due to the substrate clamping.²¹ Most of the static or

quasi-static techniques such as cantilever deflection,²¹ laser interferometry⁸⁵ and atomic force microscopy⁸⁶ provide the effective piezoelectric coefficients through the measurement of the displacement of the film or the thickness change of the sample (from the top surface of the film to the bottom surface of the substrate) instead of the strain in the film.⁸⁸ To understand the experimental measurements, we studied the total piezoresponse of a film/substrate couple, including changes of thickness of the film and the substrate, as well as a bending deflection of the film/substrate couple.⁸⁹ The theoretical calculation shows that d_{33}^f measured through the surface displacement still depend on the substrate elastic compliances and the boundary conditions. Eq. (5.2) is correct to describe effective piezoresponse measured from the surface displacement only if the substrate boundaries are fixed as shown in Figure 5.1 (a) or if the substrate is ideally rigid without any elastic deformation.⁸⁹

5. 2: Thin film/substrate couple

For a two-layer plate with a thickness much smaller than the in-plane dimension L , which consists of a piezoelectric layer with thickness h and a substrate with thickness H , Figure 5.1(b), the elastic problem on the deformation of a film/substrate couple becomes one-dimensional.⁹⁰ To elucidate the role of the substrate in the total piezodisplacement, we choose a simple case commonly used in experiments and applications: the thin film has a tetragonal structure with the polarization along c axis normal to the film, and it is epitaxially oriented on the cubic substrate layer.

The out-of-plane stress of the film is zero due to the conditions of no traction and free top surface. The in-plane stresses of the film and substrate are

$$\begin{aligned}\sigma_{11}^f &= \sigma_{22}^f = G^f (\bar{\varepsilon} + kz - d_{31}E) \\ \sigma_{11}^s &= \sigma_{22}^s = G^s (\bar{\varepsilon} + kz)\end{aligned}, \quad (5.3)$$

where the planar elastic modulus of the film and/or substrate is $G^{f,s} = 1/(S_{11}^{f,s} + S_{12}^{f,s})$, the superscripts f and s stands for the film and the substrate respectively, $\bar{\varepsilon}$ and k are the average strain and the curvature. The constants $\bar{\varepsilon}$ and k can be determined by the requirement that both the average internal stress and the average momentum of internal stress should be equal to zero:

$$\int_{-(H+h)/2}^{+(H+h)/2} \sigma(z) dz = 0 \quad \text{and} \quad \int_{-(H+h)/2}^{+(H+h)/2} z \sigma(z) dz = 0. \quad (5.4)$$

The solution of Eq. (5.4) is

$$\begin{aligned}k &= 12d_{31}E\alpha(1-\alpha)\gamma / HN, \\ \bar{\varepsilon} &= \alpha d_{31}E \{ [1 - (1-2\alpha)^3] + \gamma [1 + (1-2\alpha)^3] - 6\alpha(1-\alpha)^2(1-\gamma) \} / N.\end{aligned} \quad (5.5)$$

where $N = [\alpha + (1-\alpha)\gamma] \{ [1 - (1-2\alpha)^3] + \gamma [1 + (1-2\alpha)^3] \} - 6\alpha^2(1-\alpha)^2(1-\gamma)^2$,

$\alpha = h/(H+h)$ is the fraction of film in the film/substrate couple, $\gamma = G^f / G^s$ is the ratio of planar elastic modulus between the film and the substrate, and superscripts f and s stands for the film and the substrate respectively.

When the thickness of the thin film is much smaller than the thickness of the substrate ($h \ll H$), the curvature and the average strain can be simplified as⁹¹

$$\begin{aligned}k &= 6d_{31}E\alpha\gamma / H, \\ \bar{\varepsilon} &= \alpha d_{31}E\gamma.\end{aligned} \quad (5.6)$$

The limit of $\alpha \rightarrow 0$ is corresponding to a completely clamped thin film. The stress in the substrate is negligible compared with that of the film. The in-plane stress in the film is $\sigma_{11} = \sigma_{22} = -G^f d_{31}E$, therefore the out-of-plane strain in the film is

$$\varepsilon_3^f = d_{33}E - S_{13}^f(\sigma_{11} + \sigma_{22}) = d_{33}E - 2S_{13}^f G^f d_{31}E, \quad (5.7)$$

which is exactly corresponding to Eq. (5.2).

However, Eq. (5.2) is not sufficient when the surface displacement instead of the strain of the film is measured. The total displacement of the top surface of the film, u , consists of contributions from the thickness changes of both the thin film and the substrate, Δh , and the bending deflection, b .⁹²

The total thickness change Δh can be integrated from the displacements of the film and the substrate as:

$$\Delta h = d_{33}Eh + \int_{(H-h)/2}^{(H+h)/2} \frac{2S_{13}^f(\bar{\varepsilon} + kz - d_{31}E)dz}{(S_{11}^f + S_{12}^f)} + \int_{-(H+h)/2}^{(H-h)/2} \frac{2S_{13}^s(\bar{\varepsilon} + kz)dz}{(S_{11}^s + S_{12}^s)}, \quad (5.8)$$

where the in-plane strain has been transformed into the out-of-plane strain by Poisson effect. Thus the effective d_{33}^f measured through thickness change is equal to Δh divided by Eh (voltage):

$$d_{33}^f = d_{33} - \frac{2d_{31}S_{13}^f}{(S_{11}^f + S_{12}^f)} + \frac{2d_{31}S_{13}^s}{(S_{11}^s + S_{12}^s)}\gamma, \quad (5.9)$$

where the first term on the right side is the intrinsic piezodeformation of a free-standing film, the second term is a negative contribution due to the clamping effect, and the last term is an additional positive contribution due to the elastic deformation of the substrate because the compliance S_{13}^s has a negative value generally. It also proves that Eq. (5.2) is correct to describe the effective piezoresponse based on the thickness change of the film if the substrate boundaries are fixed as in Figure 5. 1(a) or if the substrate is ideally rigid, where the contribution from the substrate disappears.

In general, Eq. (5. 9) demonstrates that the elastic deformation of the substrate contributes to the total thickness change of the film/substrate couple and partially compensates the effect of clamping imposed by the substrate: 1) If the elastic properties of the substrate are same with that of the thin film, $S_{13}^s = S_{13}^f$, the elastic deformation of substrate exactly compensates the clamping effects of the thin film, which means that the total thickness change of the film/substrate couple is equal to the thickness change of the film without constraint; 2) The substrate elastic deformation may exceed the clamping effect if a substrate is much softer than the film, $|S_{13}^s| > |S_{13}^f|$, which means that the third term on the right side of Eq. (5. 9) becomes much larger than the second term. Therefore even if a film which is thinner than a substrate, the total displacement of the film on the substrate still depends on the elastic properties of the substrate.

The bending of the film/substrate couple leads to a deflection⁹³ that is considerably large if the in-plane size of a substrate or a film, L , is much larger than the thickness of the substrate, H . When $h \ll H$, the curvature of the bending is described as $1/\rho = k = 6hd_{31}E\gamma / H^2$ (Eq. (5.6)), which corresponds to the commonly used Stoney approximation. The bending deflection is

$$b = \frac{(L/2)^2}{2\rho} = \frac{3hd_{31}E\gamma}{4} \left(\frac{L}{H} \right)^2, \quad (5.10)$$

which depends on the square of the substrate aspect ratio L/H . Thus for $L/H > 10$, the bending contribution to the surface displacement of the film/substrate couple can be more than an order of magnitude greater than the intrinsic piezoelectric effect of the film. Note that the bending deflection results in a displacement that has an opposite

sign with the electric field induced displacement of the film, because $d_{31}E$ is negative when $d_{33}E$ is positive. Therefore, the effective piezoelectric coefficient can be much less than the fully clamped one predicted by Eq. (5.2) or can even have a large negative value if the piezoresponse is measured through the surface displacement.

For a symmetrical three-layer stack consisting of two piezoelectric thin films and an inactive substrate layer, as illustrated in the left part of Figure 5.1(c), the bending is eliminated.⁹⁴ When $h \ll H$, the film/substrate couple with fixed bottom surface (right) can be treated as a symmetrical case (left) as shown in Figure 5.1(c). The effective d_{33}^f measured through the total thickness change in the symmetrical case coincides with Eq. (5.9). It means that the effective d_{33}^f measured through the thickness change of the bent film/substrate couple is equal to the thickness change of the film/substrate couple with a fixed bottom surface.

5.3: Conclusion

Theoretical analysis based on different boundary conditions has demonstrated that the effects of the substrate contribution play a significant role in the converse piezoelectric response of the piezoelectric thin film on a substrate and therefore cannot be neglected. The elastic deformation of the substrate contributes positively to the total piezodisplacement. But the film/substrate bending can give much larger negative deflections.

Chapter 6: Summary

The thermodynamic study gives a theoretical explanation of nonlinear electric field dependence of intrinsic piezoelectric properties in single domain PZT crystal and epitaxial film. There are two regimes of the nonlinear behavior. In the relatively small field, linear electric field dependence in bulk single crystal and thin films is effective. Beyond this electric field range, more dramatic nonlinear relationship of electric field dependence dominates the change of piezoelectric properties. It is shown that the tunability is sensitive to misfit, thus it is possible to get different electric field tunabilities by adjusting misfits. The tunability can be controllable and enhanced through strain engineering that has been reported dramatically increased ferroelectric qualities of epitaxial thin films.

The elastic interactions between 180° ferroelectric domains under an external electric field has been introduced and explained. The effects on the dielectric and piezoelectric response of 180° ferroelectric thin films including intrinsic and extrinsic contributions are calculated and presented. The extrinsic contributions are notable and can be used to explain the characteristics in dielectric and piezoelectric hysteresis loops are explained for a thin film consisted of 180° ferroelectric domains. We should know the differences between the coercive fields measured from ferroelectric hysteresis loops and piezoelectric ones.

The elastic energy of piezostress is a considerable contribution in the thermodynamics of switching domain under electric field, particularly for thin films under large electric field. The relaxation of piezostress is essential even if it is not a controlling factor in the switching of 180° domains in thin films. The analysis of

numerical values included in the criterion of twinning relaxation shows that ferroelectric materials with special relation between the electrical and mechanical parameters are available for such a kind of relaxation. Therefore the further investigations of twinning relaxation as well as other mechanism of stress relaxation become a necessary step for the full understanding of the polarization switching in ferroelectric films.

Theoretical analysis based on different boundary conditions has demonstrated that the effects of the substrate contribution play a significant role in the converse piezoelectric response of the piezoelectric thin film on a substrate and therefore cannot be neglected. The elastic deformation of the substrate contributes positively to the total piezodisplacement. But the film/substrate bending can give much larger negative deflections

The results obtained are very important for the applications of piezoelectric devices and memory devices based on ferroelectric thin films. Especially, when the thickness of high quality thin film can be as small as several nanometers, the effects of the high field on the piezoresponse considered in this dissertation should be taken account.

Appendix: Piezoresponse Force Microscopy

Atomic Force Microscopy^{95,96} was introduced in mid 1980s, developed quickly and get widely used since then to study the many physical, mechanical and chemical properties of the surfaces. Within various modes^{97,98} of AFM, there are still different techniques good for domain imaging include Electric Force Microscopy,⁹⁹ Scanning Surface Potential Imaging,¹⁰⁰ Scanning Capacitance Microscopy¹⁰¹ and Piezoresponse force Microscopy⁶⁴⁻⁶⁹ for imaging polarization vectors. Here we stressed on piezoresponse force microscopy, which we used in our experiments to measure electromechanical responses and get domain images. The principle is based on lock-in amplification, which led to an understanding of quantitative mapping of the electromechanical constants in thin piezoelectric materials.

The principle of the piezoresponse technique is illustrated in Figure A.1. The technique is based on the detection of the converse piezoelectric effect in ferroelectric thin films when probed using an alternating current (ac) field. This response leads to a change in the film thickness, the sign of which depends on the polarization vector direction. Thus, regions of film with opposite polarization (as illustrated in A.1 (a) and (b)) will vibrate out of phase by 180 degree (Figure A.1(c)) upon the action of this ac field. The amplitude and phase of the film vibration give an estimate of the magnitude and sign of the piezoelectric coefficient and hence that of the local polarization. Application of a direct current (dc) voltage to the tip allows the writing of domain states. A small ac field was superimposed on the dc field to read the

domain states. Thus a hysteresis loop can be traced out by plotting the vibration signal of the tip as a function of the write voltage. For the piezoresponse images the signal of *amplitude times cos(phase)* was used to plot out the spatial distribution of the polarization vectors.

On the other hand, the conductive coating on the AFM tip allows the application of dc bias to the capacitor thereby allowing the measurement of a hysteresis style loop. The schematic illustration of the AFM setup for measurement of piezoelectric constants in thin ferroelectric films is illustrated in Figure A.2. Quantification and calibration of electromechanical constants were performed in a standard quartz single crystal (Figure A.3). Thus d_{33} for the measured film is then calculated as

$$d_{33} = \frac{\text{Lock in reading (comp. units, from } d_{33} \text{ measured.)} * d_{11} \text{ quartz}}{\text{Slope (conver. const.)} * V_{ac} \text{ used to acquire the } d_{33} \text{ loop}}$$

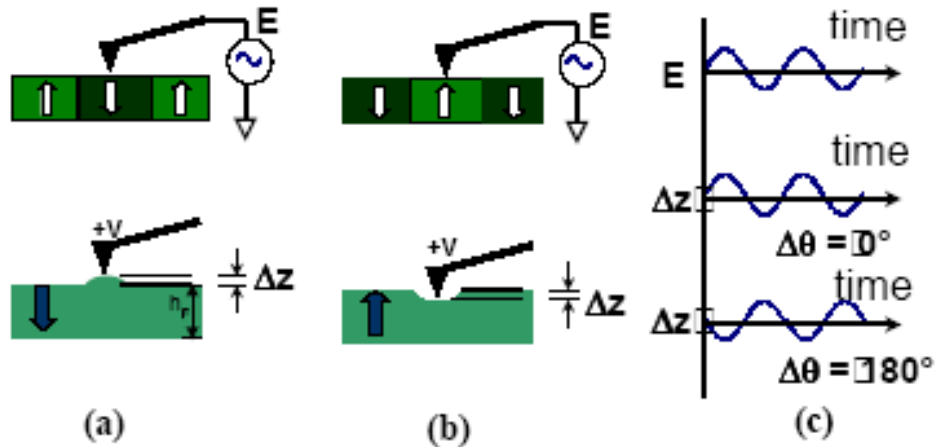


Figure A. 1: Schematic illustration of the principle behind piezoresponse microscopy. Domains poled oppositely (a) and (b) vibrate out of phase for the same sinusoidal input (c)(Adapted from Ref. 98).

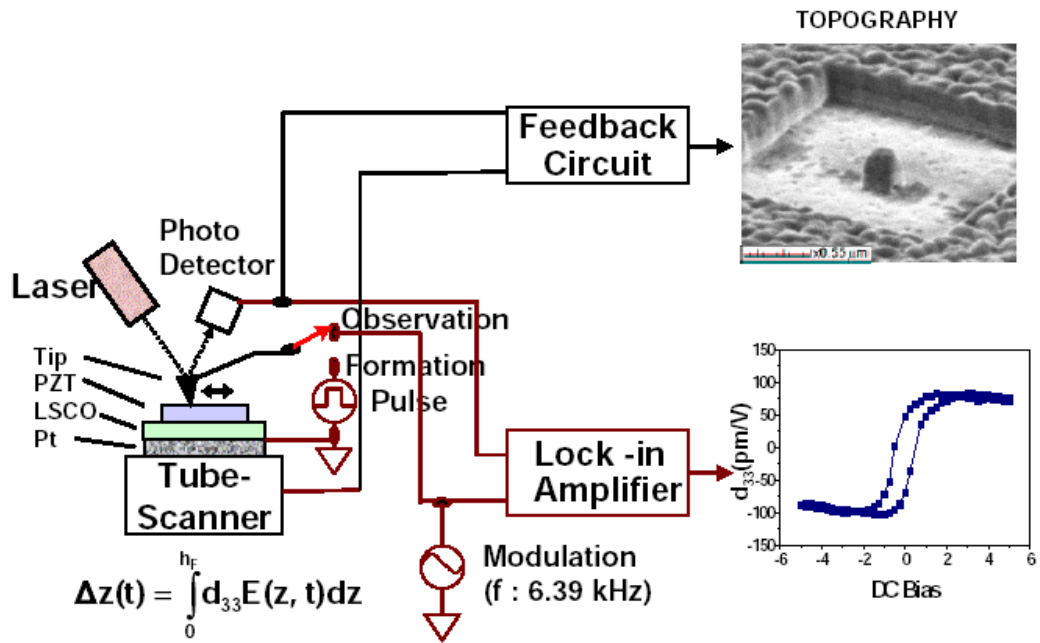


Figure A.2: Schematic of the AFM setup for measuring piezoelectric constants in ferroelectric thin films.

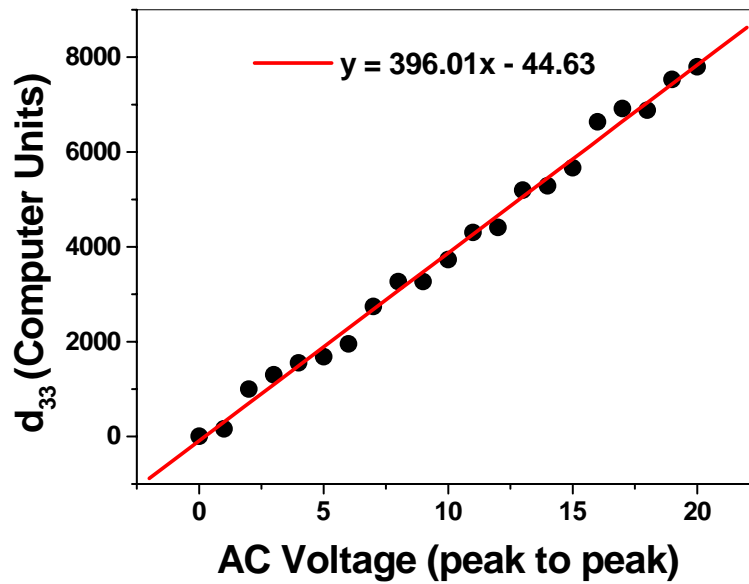


Figure A.3: Calibration of electromechanical constants with X-cut quartz.

List of Publications

1. **L. Chen**, V. Nagarajan, R. Ramesh, A. L. Roytburd, Journal of Applied Physics, **94**, 2157 (2003), “Nonlinear electric field dependence of piezoresponse in epitaxial ferroelectric lead zirconate titanate thin films.”
2. **L. Chen**, J. Ouyang, C. S. Ganpule, V. Nagarajan, R. Ramesh, and A. L. Roytburd, Applied Physics Letters, **84**, 254 (2004), “Formation of New 90° Elastic Domains During Local 180° Switching In Epitaxial Ferroelectric Thin Films”.
3. **L. Chen**, J. Li, J. Slutsker, J. Ouyang and A. L. Roytburd, Journal of Materials Research, **19**, 2853(2004) “Contribution of substrate to converse piezoelectric response of constrained thin films.”
4. J.-H. Li, **L. Chen**, V. Nagarajan, R. Ramesh and A. L. Roytburd, Applied Physics Letters, **84**, 2626(2004) “Finite-element modeling of piezoresponse in nanostructured ferroelectric films.”
5. V. Nagarajan, A. Stanishevsky, S. Prasertchoung, T. Zhao, **L. Chen**, J. Melngailis, A. Roytburd and R. Ramesh, Nature Materials **2**, 43(2003), “Dynamics of ferroelastic domains in ferroelectric thin films.”
6. V. Nagarajan, A. Stanishevsky, **L. Chen**, T. Zhao, B.T.Liu, J. Melngailis, A. L. Roytburd and R. Ramesh, Applied Physics Letters, **81**, 4215(2002), “Realizing intrinsic piezoresponse in epitaxial sub-micron Lead zirconate titanate capacitors on Si.”

7. J. Ouyang, S. Y. Yang, **L. Chen**, A. L. Roytburd, and R. Ramesh, Applied Physics Letters, **85**, 278(2004) “Crystal orientation dependence of the longitudinal converse piezoelectric properties for epitaxial single domain ferroelectric films.”
8. **L. Chen**, J. Ouyang, Z. Ma, and A. L. Roytburd. (In preparation) “180° elastic ferroelectric domains under electric field.”
9. Z. Ma, **L. Chen**, J. Ouyang, F. Zavaliche, T. Zhao J. Li, A. Roytburd, J. Melngailis, R. Ramesh. (In preparation) “ External piezoelersponse of ferroelastic domains in $\text{PbZr}_{0.2}\text{Ti}_{0.8}\text{O}_3$ heterostructures on Si substrate”

REFERENCES

1. T. Ikeda, *Fundamentals of piezoelectricity*, Oxford University Press, 1990.
2. W. G. Cady, *Piezoelectricity*, Dover Publications, Inc. 1964.
3. J. F. Nye, *Physical properties of crystals*, Oxford University Press Inc., New York, 1985.
4. M. E. Lines and A. M. Glass, *Principles and applications of ferroelectrics and related materials*, Clarendon Press, Oxford, 1977.
5. Franco Jona and G. Shirane, *Ferroelectric crystals*, Dover Publications Inc., New York, 1993.
6. B. A. Stokov and A. P. Levanyuk, *Ferroelectric phenomena in crystals: Physical foundations*, Springer Verlag, Berlin Heidelberg, 1998.
7. Orlando Auciello, James F. Scott, and Ramamoorthy Ramesh, *Physics Today*, p22, July 1998.
8. James F. Scott and Carlos A. Paz De Araujo. *Science*, 246, 1400 (1989).
9. S. Li, W. Cao, and L. E. Cross, *J. Appl. Phys.* 69, 7219(1991).
10. G. Arlt and H. Dederichs, *Ferroelectrics* 29, 47(1980).
11. O. Boser, *J. Appl. Phys.* 62, 1344 (1987).
12. V. Perrin, M. Troccaz, and P. Gonnard, *J. Electroceram.* 4, 189 (2000).
13. V. Mueller and Q. M. Zhang, *Appl. Phys. Lett.* 72, 2692 (1998).
14. V. Mueller and Q. M. Zhang, *J. Appl. Phys.* 83, 3754 (1998).

15. G. Robert, D. Damjanovic, N. Setter, and A.V. Turik, *J. Appl. Phys.* 89, 5067 (2001).
16. Na Sai, Karin M. Rabe and David Vanderbilt, *Phys Rev B* 66, 104108(2002).
17. K. Choi, M. Biegalski, Y.Li, A. Sharan, J. Schubert, R. Uecker, P. Reiche, Y.B. Chen, X. Pan, V. Gopalan, L. -Q. Chen, D. G. Schlom, and C. B. Eom, *Science*, 306, 1005 (2004).
18. H. Haeni, P. Irvin, W. Chang, R. Uecker, P. Reiche, Y. L. Li, S. Choudhury, W. Tian, M. E. Hawley, B. Craigo, A. K. Tagantsev, X. Q. Pan, S. K. Streiffer, L. Q. Chen, S. W. Kirchoefer, J. Levy, D. G. Schlom, *Nature*, 430, 758 (2004).
19. N. A. Pertsev and V. G. Koukhar, *Appl. Phys. Lett.*, 77, 2596 (2000).
20. V. G. Koukhar, N. A. Pertsev and R. Waser, *Phys. Rev. B.* 64, 214103 (2001).
21. A. L. Kholkin, Ch. Wuthrich, D. V. Taylor, and N. Setter, *Rev. Sci. Instrum.* 67, 1935 (1996).
22. H. Maiwa, J. A. Christman, S-H kim, D-J Kim, J-P Maria, B. Chen, S. K. Streiffer and A. I. Kingon, *Jpn. J. Appl. Phys.* 38, 5402 (1999).
23. H. Maiwa, J. P. Maria, J. A. Christman, S. H. Kim, K. Streiffer, and A. I. Kingon, *Intgr. Ferroelectrics* 24, 139-146 (1999).
24. S. Buhlmann, B. Dwir, J. Baborowski, P. Muralt, *Appl. Phy. Lett.* 80, 3195(2002).
25. V. Nagarajan, A. Stanishevsky, L. Chen, T. Zhao, B. -T. Liu, J. Melngalis, A. L. Roytburd, and R. Ramesh, J. Finder, Z. Yu, R. Droopad, and K. Eisenbeiser, *Appl. Phy. Lett.* 81, 4215(2002).

26. O. Kuffer, I. Maggio-Aprile, J.-M. Triscone, and Q. Fischer and Ch. Renner
Appl. Phys. Lett. 77, 1701(2000).
27. L. Chen, V. Nagarajan, R. Ramesh, A. L. Roytburd, J. Appl. Phys., 94, 5147
(2004).
28. M. J. Haun, E. Furman, S. J. Jang, and L. E. Cross, Ferroelectrics 99,
45(1989).
29. M. J. Haun, E. Furman, S. J. jang, H. A. Mckinstry, and L. E. Cross, J. Appl.
Phys. 62, 3331(1987).
30. Landolt-Börnstein, *Numerical Data and Functional Relationships in Science
and Technology*, edited by K.-H. Hellwege and A. M. Hellwege Springer,
Berlin, 1981, Vol. 16.
31. K. Lefki and G. J. M. Dormans, J. Appl. Phys. 76, 1764 (1994).
32. B. Jaffe, W. R. Cook, and H. Jaffe, *Piezoelectric Ceramics*, Academic,
London, 1971.
33. A. L. Roytburd, S. P. Alpay, V. Nagarajan, C. S. Ganpule, S. Aggarwal, E. D.
Williams, and R. Ramesh, Phys. Rev. Lett. 85, 190 (2000).
34. G. Gavriyachenko and E. G. Fesenko, Sov. Phys. Crystallography. 16, 549
(1971).
35. A. V. Turik, E. G. Fesenko, V. G. Gavriyachenko, and G. I. Khasabova, Sov.
Phys. Crystallogr. 19, 677 (1975)
36. A. V. Turik, N. B. Shevchenko, V. G. Gavriyachenko, and E. G. Fesenko,
Phys. Status Solidi B 94, 525 (1979).

37. Z. Li, M. H. Grimsditch, X. Xu, and S-K. Chan, *Ferroelectrics* 141, 313 (1993).
38. A. G. Kalinichev, J. D. Bass, B. N. Sun and D. A. Payne, *J. Mater. Res.* 12, 2623 (1997)
39. K. M. Rabe and E. Cockayne, in *First-principles Calculations for Ferroelectrics: Fifth Williamsburg Workshop*, edited by R. E. Cohen, AIP, 1998, vol. 436, pp. 61–70.
40. E. Heifets and R. E. Cohen, *AIP Conf. Proc.* 626, 150 (2002).
41. S. K. Streiffer, J. A. Eastman, D. D. Fong, C. Thompson, A. Munkholm, M. V. Ramana Murty, O. Auciello, G. R. Bai, and G. B. Stephenson, *Phys. Rev. Lett.* 89, 067601 (2002).
42. D. D. Fong, G. B. Stephenson, S. K. Streiffer, J.A. Eastman, O. Auciello, P. H. Fuoss, and C. Thompson, *Science*, 304, 1650(2004).
43. M. E. Drougard and D. R. Young, *Phys. Rev.* 94,1561(1954).
44. A. K.Tagantsev, P. Muralt, and J. Fousek, *Mat. Res. Soc. Symp. Proc. Vol.* 784, C.10.6. (2004).
45. L. Chen, J. Ouyang, C. S. Ganpule, V. Nagarajan, R. Ramesh, and A. L. Roytburd, *Appl. Phys. Lett.* 84, 254(2004).
46. A. L. Roitburd, *Phys. Status. Solidi. A* 37, 329 (1976)
47. S. Kwak et al, *Phys. Rev. Lett.* 68, 3733 (1992),
48. S. Kwak et al, *Phys. Rev. B.* 49, 14865(1994).
49. W. Pompe et al, *J. Appl. Phys.* 74, 6012(1993);
50. J. S. Speck et al. *J. Appl. Phys.* 76, 466(1994),

51. J. S. Speck et al. J. Appl. Phys. 78, 1696(1995).
52. A. L. Roytburd, J. Appl. Phys. 83, 228(1998),
53. A. L. Roytburd, J. Appl. Phys. 83, 239(1998).
54. N. Sridhar, J. M. Rickman, and D. J. Srolovitz, Acta. Mater. 44, 4085(1996);
55. N. Sridhar, J. M. Rickman, and D. J. Srolovitz, Acta. Mater. 44, 4097(1996).
56. Kagner et al, Phys. Rev. Lett. 85, 341 (2000).
57. Kagner et al, Phys. Rev. B. 66, 045305 (2002).
58. A. M. Bratkovsky and A..P. Levanyuk, Phys. Rev. Lett. 86, 3642 (2001).
59. A. M. Bratkovsky and A..P. Levanyuk, Phys. Rev. B. 65, 094102(2002).
60. V. Nagarajan et al., Appl. Phys. Lett. 84, 5225 (2004)
61. A. V. Bune, V. M. Fridkin, Stephen Ducharme, L. M. Blinov, S. P. Palto, A. V. Sorokin, S. G. Yudin, A. Zlatkin, Nature 391, 874 (1998).
62. Stephen Ducharme, V. M. Fridkin, A. V. Bune, S. P. Palto, L. M. Blinov, N. N. Petukhova, and S. G. Yudin, Phys. Rev. Lett. 84, 175(2000).
63. L. Lian and N. R. Sottos., J. Appl. Phys, 87, 3941(2000).
64. O. Kolosov, A. Gruverman, J. Hatano, K. Takahashi, and H. Tokumoto, Phys. Rev. Lett., 74, 4309 (1995).
65. T. Tybell, C. H. Ahn, and J. -M. Triscone, Appl. Phys. Lett. 72, 1454 (1998).
66. C. S. Ganpule, V. Nagarajan, H. Li, A. S. Ogale, D. E. Steinhauer, S. Aggarwal, E. Williams, R. Ramesh and P. De Wolf, Appl. Phys. Lett. 77, 272(2000).
67. A. Gruverman, A. Kholkin, A. Kington and H. Tokumoto, Appl. Phys. Lett. 78, 2751(2001).

68. C. Durkan, M. E. Welland, D. P. Chu, and P. Miglirato, *Phys. Rev. B.* 60, 16198 (1999).
69. S. V. Kalinin and D. A. Bonnell, *Phys. Rev. B.* 65,125408 (2002).
70. M. Molotskii, *J. Appl. Phys.* 93, 6234(2003),
71. E. J. Mele, *Am. J. Phys.* 69, 557(2001).
72. A. L. Roytburd, “*Martensitic Transformation as a Typical Phase Transformation in Solids,*” in *Solid State Physics*, 33, Academic Press, (1978), P. 317
73. A. Roytburd, *Phase Transitions* 45, 1 (1993).
74. A. G. Khachaturyan, *Theory of Structural Transformations in Solids*, John Wiley & Sons, New York, 1983.
75. A.L. Roytburd and Y. Yu in *Twinning in Advanced Materials*, eds. M.H. Yoo and M. Wuttig, (TMS, 1994) vol. 221, p.217.
76. N. A. Pertsev and A. Yu. Emelyanov, *Appl. Phys. Lett.*, 71, 3646 (1997)
77. M. Kolkin, P. Muralt and N. Setter, *Appl. Phys. Lett.*, 72, 3217 (1998)
78. K. S. Lee, Y. K. Kim, S. Baik, J. Kim and I. S. Jung, *Appl. Phys. Lett* 79, 2444 (2002)
79. S. P. Alpay and A. L. Roytburd, *J. Appl. Phys.* 83,4714 (1998).
80. J. Slutsker, A. Artemev and A. L. Roytburd, *J. Appl. Phys.* 91, 9049 (2002)
81. A. L. Roytburd, S. P. Alpay, L. A. Bendersky, V.Nagarajan and R. Ramesh, *J. Appl. Phys.*, 89, 553 (2001).
82. V. Nagarajan, A. Roytburd, A. Stanishevsky, S. Prasertchoung, T. Zhao, L. Chen, J. Melngailis and R. Ramesh, *Nature Materials* 2, 43(2003).

83. C. S. Ganpule, A. L. Roytburd, B. K. Hill, V.Nagarajan, E. D. Williams, R. Ramesh and J. F. Scott, *Phys. Rev. B* 65, 014101 (2002).
84. F. Xu, F. Chu, and S. Trolier-McKinstry, *J. Appl. Phys.* 86, 588 (1999).
85. M. A. Dubois and P. Muralt, *Sens. Actuators A* 77, 106 (1999).
86. J. A. Christman, R. R. Woolcott, A. I. Kingon, and R. J. Nemanich, *Appl. Phys. Lett.* 73, 3851 (1998).
87. S. Buhlman, B. Dwir, J. Baborowski, and P. Muralt, *Appl. Phys. Lett.* 75, 3195 (2002).
88. J.-H. Li, L. Chen, V. Nagarajan, R. Ramesh and A. L. Roytburd, *Appl. Phys. Lett.* 84, 2626 (2004).
89. Lang Chen, J. Li, J. Slutsker, J. Ouyang and A. L. Roytburd, *J. Mater. Res.* 19, 2853 (2004)
90. A. L. Roytburd and J. Slutsker, *Mater. Trans.* 43, 1023 (2002).
91. M. Finot, and S. Suresh, *J. Mech. Phys. Solids*, 44, 683 (1996).
92. R. Steinhausen, T. Hauke, W. Seifert, V. Müller, H. Beige, S. Seifert and P. Löbmann, *Proceedings of the 11th IEEE ISAF 98*, p 93 (1998).
93. A. Barzegar, D. Damjanovic, N. Ledermann, and P. Muralt, *J. Appl. Phys.* 93, 4756 (2003).
94. A. L. Roytburd, *Integr. Ferroelectr.* 38, 119 (2001).
95. G. Binnig, C. F. Quate, and Ch. Gerber, *Phys. Rev. Lett.* 56, 930(1986).
96. G. Binnig, H. Rohrer, Ch. Gerber, and E. Weibel, *Phys. Rev. Lett.* 50, 120 (1983).

97. Digital Instruments. Scanning probe microscopy training notebook. Veeco Metrology Group, August 1998.
98. C. S. Chandan, PhD thesis, University of Maryland, 2001.
99. M. Labardi, V. Likodimos, and M. Allegrini, *Phys. Rev. B*, 61, 14390 (2000).
100. S. V. Kalinin and Dwan A. Bonnell, *Phys. Rev. B*, 62, 10419 (2000)
101. J. J. Kopanski, J. F. Marchiando, and D. W. Berning, *J. Vac. Sci. and Tech. B*, 16, 339(1998).

Glossary of Notations

- α : The 1st modified coefficient of free energy expansions (Chapter 2); domain volume fraction (Chapters 3 and 4); Volume fraction (Chapter 5)
- β : The 2nd modified coefficient of free energy expansions
- γ : The 3rd modified coefficient of free energy expansions (Chapter 2); the ratio of d_{31} and d_{33} (Chapter 4); the ratio of planar elastic modulus between the film and the substrate (Chapter 5)
- ν : Poisson ratio
- a_1, a_{11}, a_{111} : Ferroelectric dielectric stiffness at constant stress
- b : Bending deflection; stands for bulk materials case or free standing film
- f : Stands for constrained film case
- h : Thickness of film
- H : Thickness of substrate
- L : Length of film/substrate
- k : Average curvature
- E : Electric field strength
- E_c : Coercive electric field
- E_{th} : Thermodynamic coercive electric field
- P : Polarization
- P_s : Spontaneous polarization
- p : Electric field induced polarization
- D : Electrical displacement; the width of domain period

T_c : Curie temperature

F : Free energy

σ_{ij} ($i, j = 1-3$): Stress components

ε_{ij} ($i, j = 1-3$): Strain components

d_{ij} ($i = 1-3, j = 1-6$): Piezoelectric coefficients

S_{ij} ($i = 1-6, j = 1-6$): Elastic compliances components

Q_{ij} ($i = 1-6, j = 1-6$): Electrostrictive coupling between the ferroelectric polarization and stress

χ, χ_{ij} : Dielectric susceptibility